Cell Calcium 117 (2024) 102834

Contents lists available at ScienceDirect

Cell Calcium

journal homepage: www.elsevier.com/locate/ceca

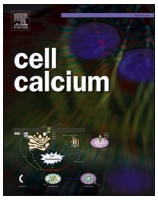

Development of chemical tools based on GSK-7975A to study store-operated calcium entry in cells

Dominic Tscherrig [a,1,2], Rajesh Bhardwaj [b,*,1,3], Daniel Biner [c], Jan Dernič [b,4], Daniela Ross-Kaschitza [a], Christine Peinelt [a], Matthias A. Hediger [b,*], Martin Lochner [a,*]

[a] Institute of Biochemistry and Molecular Medicine, University of Bern, Bühlstrasse 28, 3012 Bern, Switzerland
[b] Department of BioMedical Research, University of Bern and Department of Nephrology and Hypertension, Inselspital, Bern University Hospital, Freiburgstrasse 15, 3010 Bern, Switzerland
[c] Department of Chemistry, Biochemistry and Pharmaceutical Sciences, University of Bern, Freiestrasse 3, 3012 Bern, Switzerland

ARTICLE INFO

Keywords:
Store-operated calcium entry
Synthetic molecular probe
Photo-caged compound
Photo-affinity labelling
Calcium imaging assay
Patch-clamp electrophysiology

ABSTRACT

Many physiological functions, such as cell differentiation, proliferation, muscle contraction, neurotransmission and fertilisation, are regulated by changes of Ca^{2+} levels. The major Ca^{2+} store in cells is the endoplasmic reticulum (ER). Certain cellular processes induce ER store depletion, *e.g.* by activating IP_3 receptors, that in turn induces a store refilling process known as store-operated calcium entry (SOCE). This refilling process entails protein-protein interactions between Ca^{2+} sensing stromal interaction molecules (STIM) in the ER membrane and Orai proteins in the plasma membrane. Fully assembled STIM/Orai complexes then form highly selective Ca^{2+} channels called Ca^{2+} release-activated Ca^{2+} Channels (CRAC) through which Ca^{2+} ions flow into the cytosol and subsequently are pumped into the ER by the sarcoplasmic/endoplasmic reticulum calcium ATPase (SERCA). Abnormal SOCE has been associated with numerous human diseases and cancers, and therefore key players STIM and Orai have attracted significant therapeutic interest. Several potent experimental and clinical candidate compounds have been developed and have helped to study SOCE in various cell types. We have synthesized multiple novel small-molecule probes based on the known SOCE inhibitor GSK-7975A. Here we present GSK-7975A derivatives, which feature photo-caging, photo-crosslinking, biotin and clickable moieties, and also contain deuterium labels. Evaluation of these GSK-7975A probes using a fluorometric imaging plate reader (FLIPR)-Tetra-based Ca^{2+} imaging assay showed that most synthetic modifications did not have a detrimental impact on the SOCE inhibitory activity. The photo-caged GSK-7975A was also used in patch-clamp electrophysiology experiments. In summary, we have developed a number of active, GSK-7975A-based molecular probes that have interesting properties and therefore are useful experimental tools to study SOCE in various cells and settings.

Abbreviations

2-APB	2-Aminoethyl Diphenylborinate
BAPTA	1,2-Bis(*o*-aminophenoxy)ethan-*N,N,N*`,*N*`-tetraacetic acid
brsm	Based on recovered starting material
CD	Current density
CuAAC	Copper-catalysed alkyne-azide cycloaddition
DCM	Dichloromethane
DMF	Dimethylformamide
ER	Endoplasmic reticulum
ESI	Electrospray ionisation
FLIPR	Fluorometric imaging plate reader
HATU	Hexafluorophosphate azabenzotriazole tetramethyl uronium
HCD	Higher energy collisional dissociation
HRP	Horseradish peroxidase
IP_3	Inositol triphosphate

* Corresponding authors.
E-mail addresses: rajesh.bhardwaj@nih.gov (R. Bhardwaj), matthias.hediger@unibe.ch (M.A. Hediger), martin.lochner@unibe.ch (M. Lochner).
[1] These two authors contributed equally to the study.
[2] Present address: Swissmedic, Swiss Agency for Therapeutic Products, Hallerstrasse 7, 3012 Bern, Switzerland.
[3] Present address: Signal Transduction Laboratory, National Institute of Environmental Health Sciences, NIH, Durham, NC 27709, USA.
[4] Present address: Institute of Pharmacology and Toxicology, University of Zürich, Winterthurerstrasse 190, 8057 Zürich, Switzerland.

https://doi.org/10.1016/j.ceca.2023.102834
Received 7 August 2023; Received in revised form 11 November 2023; Accepted 13 November 2023
Available online 15 November 2023
0143-4160/© 2023 The Authors. Published by Elsevier Ltd. This is an open access article under the CC BY license (http://creativecommons.org/licenses/by/4.0/).

SERCA	Sarcoplasmic/endoplasmic reticulum calcium ATPase
SOCE	Store-operated calcium entry
STIM	Stromal interaction molecule
TBTA	Tris((1-benzyl-4-triazolyl)methyl)amine
Tg	Thapsigargin
THF	Tetrahydrofuran
TRP	Transient receptor potential (channel)

1. Introduction

Store-Operated Calcium Entry (SOCE) is a crucial cellular process that regulates intracellular calcium levels, playing a pivotal role in cell signalling, gene expression, proliferation, and apoptosis [1]. SOCE involves the activation of plasma membrane calcium channels of the Orai family of proteins, in response to the depletion of intracellular calcium stores, primarily the endoplasmic reticulum (ER). The ER membrane STIM proteins detect the drop in ER luminal Ca^{2+} levels and gate open the Orai channels in the plasma membrane to allow the influx of Ca^{2+} in the cells, which is used by Ca^{2+} pump to refill the stores as well as by other cellular proteins to drive numerous Ca^{2+} dependent pathways. Dysregulation of SOCE is associated with a variety of diseases, including immune disorders, myopathies, neurodegenerative diseases, cardiovascular diseases, and certain cancers [2–6]. The development of specific chemical tools to modulate SOCE is critical to understanding its dynamics and its impact in disease pathogenesis. Given that there is very limited information on the modus operandi and locus actionis of most of the SOCE modulators, there is a huge scope of engineering potent SOCE modulators to gain molecular understanding on how chemical modulators inhibit these channels [7], which can be further utilized to design even more potent compounds that can differentially modulate the channel activity.

Several small compounds have been reported as SOCE inhibitors and are available as pharmacological tools for SOCE research (Figure S1). Borinate 2-APB, one of the best characterised compounds, is still widely used, despite its ample polypharmacology [8–12] (*e.g.* also targeting transient receptor potential (TRP) channels and IP_3 receptors) and known hydrolytic and oxidation-sensitive liabilities [13,14]. In addition, as a SOCE modulator, 2-APB exhibits a bimodal concentration effect: when applied in lower concentration (<10 μM), it potentiates SOCE, whereas applied in higher concentration (>30 μM), it blocks SOCE in various cell lines [15,16]. Compound BTP2 (also called Pyr2 or YM-58,483) was one of the first heterocyclic and sub-micromolar SOCE inhibitors [17], which was also shown to have appreciable activity at some TRP channels [18]. Nevertheless, its biarylamide scaffold served as a SOCE inhibitor blueprint, which spurred significant synthetic activity in industrial and academic labs. Selective and potent SOCE inhibitors Synta66, GSK-7975A and Ro2959 were the result of these efforts and they are now preferentially used in cell-based SOCE studies in various cell lines [7,19,20]. *In vivo* experiments have demonstrated that these biarylamides tend to have poor solubility and disadvantageous pharmacokinetic properties. Very recently, Pirali and co-workers and Khedkar and co-workers have presented compounds **34** [21] and **36** [22], respectively, with significantly improved pharmacokinetic profiles and *in vivo* efficacies (Figure S1). Pyrazines CM4620 (also called Auxora) and PRCL-02 appear to be well tolerated and have entered phase II clinical trials recently, for pneumonia in COVID-19 patients [23] and acute pancreatitis [24] (CM4620), and for psoriasis [25] (PRCL-02).

Small compound SOCE modulators are valuable molecular tools in their own right, but they can also serve as platform for the development of research probes. In addition to the desired biological activity, these probes can feature useful tags, such as fluorescent dyes, biotin pull-down moieties, electrophilic or photo-crosslinking groups for covalent target modifications and "click" handles (*e.g.* azides, alkynes). These latter clickable functional groups have become valuable substituents of bioactive ligands, as they can be addressed by specific and biocompatible chemistry after covalent protein modification (*e.g.* by photo-crosslinking), for efficiently coupling useful tags (biotin, fluorescent dyes) to the modified protein. Light is a non-invasive, biocompatible reagent when used at wavelengths above 300 nm. Many molecular research probes have thus been developed that can be activated by light. These include photo-switchable [26] and photo-caged compounds [27] that can be used to initiate biological effects with temporal and spatial precision. Furthermore, photo-crosslinking probes have become an important tool in proteomic studies, and for target validation and identification [28]. In the SOCE field, Udasin *et al.* have presented photo-switchable boronic acid LOCI-1 (Figure S1), reminiscent of the known modulator 2-APB [29]. Earlier, photo-switchable CRAC channel inhibitor piCRAC-1 based on GSK-5498A was published by Zhou, Li and co-workers [30]. Both probes were also evaluated *in vivo*. Pyrazole compound Pyr3, a congener of BTP2, served as starting point to develop photo-affinity probe Pyr-PP that was utilised to identify and validate TRPC3 as its target [31].

Our research presents the development and characterisation of chemical probes based on known SOCE inhibitor GSK-7975A and highlights the scope of tolerated modifications.

2. Results and discussion

2.1. Synthesis of GSK-7975A probes

We set out with the goal of developing a synthetic strategy that will allow to efficiently generating GSK-7975A derivatives featuring modifications at either or both ends of the active scaffold. Our previously modified synthesis of the parent GSK-7975A structure [16] is too linear to serve this purpose and we decided to redesign it. Retrosynthetic analysis identified key pyrazole building block **1** to achieve this goal (Scheme S1). Selective *N*-1 alkylation of 3-nitropyrazole went smoothly and gave product **2** in very good yield (91 %). The following methyl ethyl cleavage using standard reagent boron tribromide (BBr_3) yielded complex mixtures, including boron adducts of 3-nitro pyrazole. Alternatively, *O*-demethylation was achieved by treatment with MgI_2 in ionic liquid [32] and delivered desired key building block **1** in workable 57 % yield (65 % based on recovered starting material (brsm)). At this point, the phenol moiety of the GSK-7975A skeleton can be functionalised with useful bioorthogonal handles, such as clickable alkynes and methyl ketones, in very good yields (intermediates **3b, 3c**). Subsequent reduction of the nitro group with $SnCl_2$ was very efficient (97 %-quantitative yield) and the resulting amines **4a-c** were coupled with corresponding carboxylic acids, aided by hexafluorophosphate azabenzotriazole tetramethyl uronium (HATU), to give final GSK-7975A probes **5**–**9** (Table 1). These HATU-mediated amide formations worked well (78–94 % isolated yields), except for **8**, where we observed formation of several side products and consequently recorded a very poor isolated yield (8 %). In summary, our synthetic route gave access to GSK-7975A-related probes in overall yields of up to 49 % over the five steps.

Probes **10** and **11** (Table 1) were obtained by direct *O*-alkylation of GSK-7975A in moderate yields (36–41 %, see *4.1 Chemical Synthesis*). Alternatively, Probe **9** was synthesized via a different route. 3-aminopyrazole was first amidated with 4-azido-2,3,5,6-tetrafluorobenzoic acid, followed by *N*-1 alkylation of the pyrazole with 4-methoxy-2-(trifluoromethyl)benzyl bromide and methyl ether cleavage with BBr_3 (Scheme S2). Due to the swapped probe design compared to **5**–**11** (Table 1), probe **12** was accessed using an alternative synthetic pathway. Methyl 2,6-difluoro-4-hydrobenzoate was first *O*-propargylated and directly amidated [33] with 3-aminopyrazole subsequently (Scheme S3). Finally, *N*-1 benzylation of the pyrazole ring gave final probe **12**.

The alkyne tag, as in **6, 7, 10** and **12**, is a commonly used small handle for bioorthogonal click conjugation reactions via copper-catalysed alkyne-azide cycloaddition (CuAAC, "click chemistry") [34]. To probe the compatibility with the GSK-7975A moiety and extension of the ligand at this position, we have reacted **10** with biotin azide **13**

Table 1
Chemical structures of parent GSK-7975A and synthesised probes **5**–**12**.

Compound	Structure	Compound	Structure
GSK-7975A	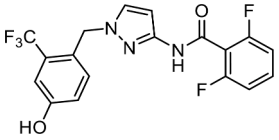	**9**	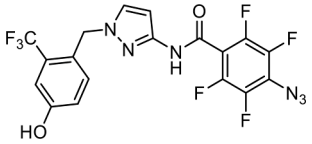
5	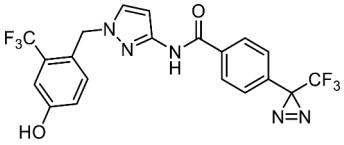	**10**	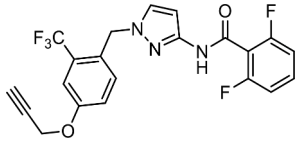
6	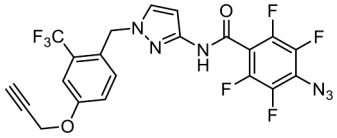	**11**	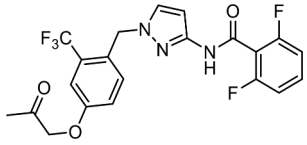
7	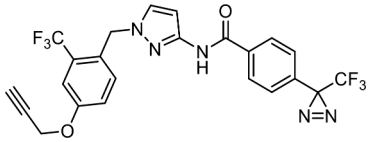	**12**	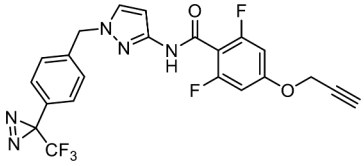
8	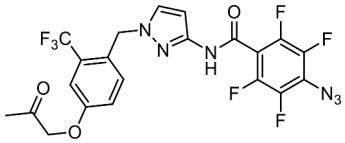		

under standard CuAAC conditions [35], delivering biotinylated **14** in acceptable yield (Scheme S4).

GSK-7975A probes **5, 7** and **12** feature photo-activatable phenyl diazirine tags that can be utilised in photo-crosslinking studies. Irradiation with near-UV light induces fragmentation of the diazirine (elimination of N_2) and generation of a highly reactive carbene that inserts into C—H or heteroatom-H bonds. This methodology can bring about covalent modification of the protein by the photo-crosslinking ligand. Subsequent analysis by protein-MS/MS can reveal the residue(s), which have been crosslinked and therefore map the binding site of the ligand. In practice, low photo-crosslinking yields for various reasons make this analysis extremely challenging. In the mixed isotope strategy, stable isotopes are introduced into the photo-crosslinking ligand and application of a 1:1-mixture of labelled and non-labelled probes in the experiment helps to identify the modified peptide peaks in the MS analysis by the isotope signature [36,37]. To this end, we have developed a synthetic route from inexpensive toluene-d_8 to access deuterated diazirine benzoic acid **15** (Scheme S5). The key step of this reaction sequence is the regioselective mono-bromination of toluene-d_8. We have adapted the procedure described by Kesling *et al.* that utilizes Faujasite NaY-type zeolite as a catalyst [38]. Activation of the zeolite catalyst by heating at 500 °C in high vacuum over two days is required to obtained high yield and exclusive *para*-substitution in the aromatic bromination to afford **16** (Table S1). This compound would be commercially available but is about 200-times more expensive than toluene-d_8. The subsequent steps leading to diaziridine **19** are standard reactions in the synthesis of phenyl diazirines and proceeded in good yields. At this point, we sought conditions to oxidize the diaziridine to the photoactive diazirine and the methyl group at the same time to obtain benzoic acid **15** in one step. Previous model experiments with non-deuterated *p*-tolyl diaziridine showed that this transformation can be efficiently achieved using $KMnO_4$ (Table S2). However, using the same reaction conditions for deuterated **19** only delivered **15** in very small amount. Further screening of other oxidation methods ultimately led to Jones conditions [39] which gave **15** in acceptable 53 % yield. It is noticeable that due to the stronger C-D bond the methyl oxidation is much slower for the deuterated substrates (Table S2). In summary, we have developed a novel synthetic pathway to obtain tetra-deuterated photo-crosslinking building block **15** in very good 28 % overall yield in six steps from inexpensive toluene-d_8. Benzoic acid **15** was finally coupled to amine **4a** and yielded the tetra-deuterated version of probe **5** (Scheme S5).

Near-UV light is a biocompatible and mild reagent and can not only be used in photo-crosslinking experiments to capture ligand-protein interactions (*e.g.* using probes **5**–**9** and **12**) but also for photo-decaging of masked modulators that then become active upon irradiation. For this reason, we have envisioned to attach a bulky, photo-cleavable group on the phenol oxygen of GSK-7975A (Scheme S6). We chose a coumarin-4-yl methyl moiety as recent reviews have pointed out its fast cleavage and suitability in biomedical applications [27,40]. Guided by similar examples in the literature [41,42] 4-methyl-7-diethylaminocoumarin (**20**) was oxidized with selenium dioxide, followed by aldehyde reduction to yield alcohol **21** (Scheme S6). The resulting alcohol group was

transformed into a chloroformate **22** and coupled with the phenol of GSK-7975A. This gave photo-caged GSK-7975A probe **23** and dimerised side product **24**, which we were not able to separate from desired **23** by chromatography (compound decomposition on silica gel or no separation using reversed phase on C_{18}-columns). Ultimately, purification by recrystallization delivered pure photo-cleavable probe **23** in 67 % isolated yield.

2.2. Activity of synthetic GSK-7975A probes on SOCE

In order to evaluate the activity of the synthetic GSK-7975A probes on SOCE and thus the impact of our structural alterations, we utilised a fluorescence-based calcium influx assay into breast cancer cells MDA-MB-231, MCF-7 or HEK293T cells, with slight modifications to the one described previously [16]. In the assay used in this work, the cells were kept in nominally Ca^{2+}-free buffer (NCF) and incubated with the compounds for 30 min. This was followed by the addition of cell-permeable SERCA inhibitor thapsigargin (Tg) and incubation for 10 min in NCF. Irreversible blocking of SERCA resulted in passive depletion of intracellular ER-stores and consequently initiated the SOCE process. Finally, extracellular $CaCl_2$ was added and external Ca^{2+} entry through CRAC channels measured by an intracellular Ca^{2+}-sensitive fluorescent dye (Fig. 1A).

Quantification of Ca^{2+} influx through CRAC channels in the presence of various concentrations of GSK-7975A showed that full block is achieved at 10 μM (Fig. 1B).

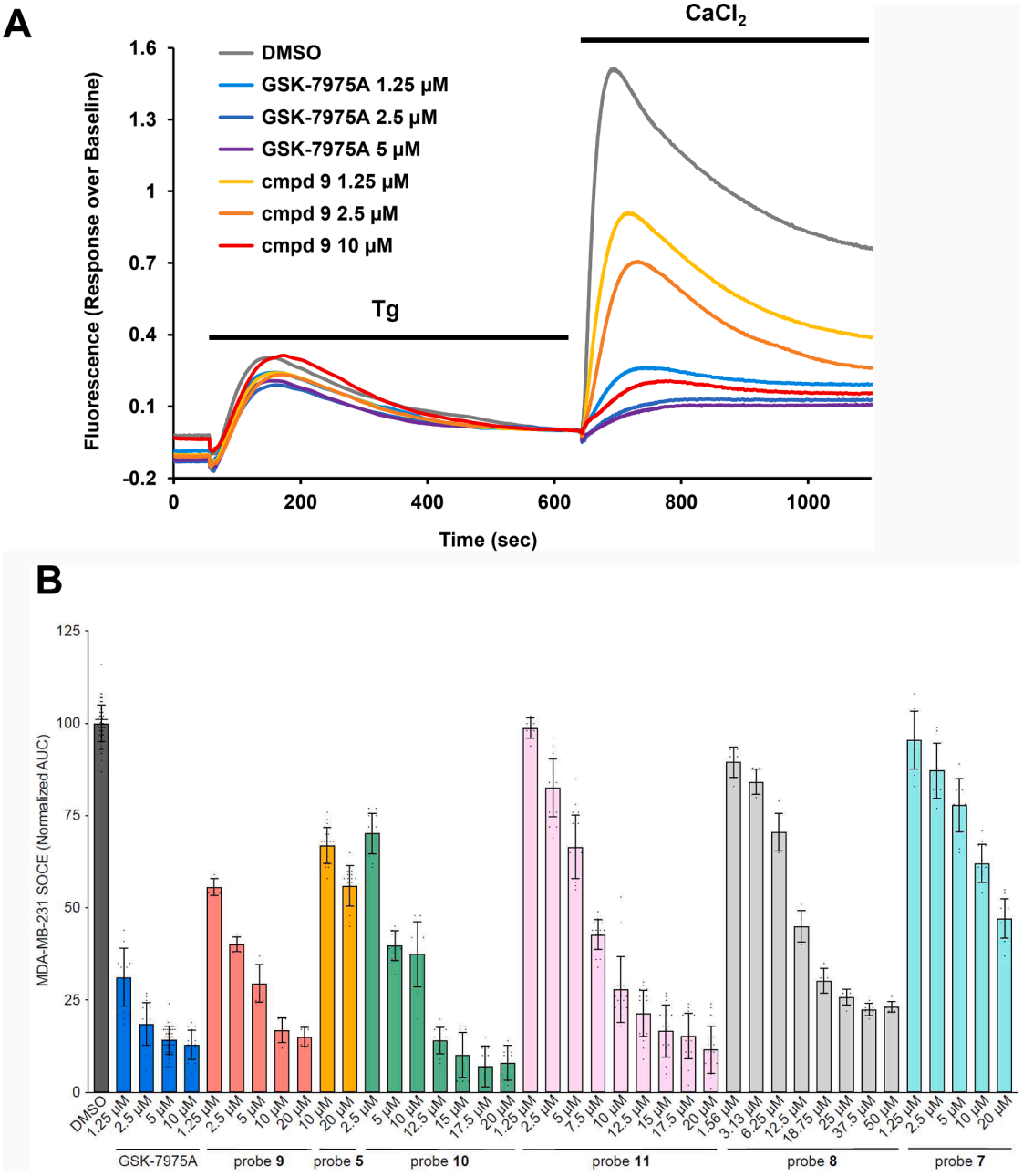

Fig. 1. Pharmacological characterisation of probes **5** and **7**–**11** regarding modulation of store-operated Ca^{2+} entry (SOCE) into mammalian cells by fluorometric imaging plate reader (FLIPR) assay. (**A**) Representative fluorescent intracellular Ca^{2+} signal recordings over the course of the assay in MDA-MB-231 cells. Black bars above traces indicate duration of reagent applications. Cells were incubated with the compound at different concentrations (30 min) in nominal Ca^{2+}-free buffer (NCF), followed by addition of thapsigargin (Tg, 1 μM, 10 min). Finally, extracellular $CaCl_2$ (2 mM) was added. (**B**) Quantification of Ca^{2+} influx after $CaCl_2$ application (area under the curve (AUC)) in the presence of GSK-7975A and its derivatives normalised to negative control (0.1 % DMSO). Data shown are mean ± SD.

Replacement of the eastern 2,6-difluorophenyl ring of GSK-7975A, as in **5** and **9** was tolerated and did not abolish the blocking effect. Whereas **9** with the azidotetrafluorophenyl moiety blocked SOCE at 10 μM as efficiently as the parent compound GSK-7975A, the slightly larger trifluoromethyldiazirinephenyl group of **5** had a stronger impact, significantly reducing SOCE inhibition about 4-fold. Regarding the western modification of the phenolic OH group of GSK-7975A with bio-orthogonal reporter handles (probes **10** and **11**), we found that they were apparently less well tolerated than the eastern ring modifications (**9**). A compound concentration of 15 μM or higher was required for **10** and **11** to obtain maximal Ca^{2+} influx inhibition, compared to the parent compound. Between the two western modifications, the more linear alkyne group (**10**) had a smaller influence on the SOCE blocking property than the ketone (**11**).

Interestingly, when combining the most tolerated modifications at both ends of the parent GSK-7975A ligand in probe **6**, no more than 50 % inhibition could be recorded, even at concentrations as high as 50 μM (Figure S2). For bifunctionalised GSK-7975A probes it was more beneficial with respect to SOCE blocking activity to combine the western alkyne handle with the eastern diazirinephenyl photo-crosslinking group (**7**) or the western ketone reporter group with the eastern azidophenyl crosslinker (**8**). Between these two, the latter probe **8** showed slightly higher SOCE blocking activity (Fig. 1B). Ultimately, bifunctionalised **8** was only about 3–5 times less active than parent GSK-7975A and reached maximum block at about 30 μM concentration. We explored if swapping of western reporter tag and eastern photo-crosslinking moiety makes a significant impact on SOCE blocking activity. To this end, we synthesised inverted probe **12** (Table 1). In comparison to its congener probe **7**, inverted **12** was slightly more active in blocking SOCE (Fig. 2) at concentrations of 10 μM or higher. Compared to unsubstituted parent GSK-7975A swapped probe **12** showed only about three times reduced inhibitory activity at 10 μM concentration.

Extending the GSK-7975A scaffold by clicking a large biotin affinity tag to the western position (probe **14**) completely abolished SOCE inhibition activity, compared to the unconjugated alkyne probe **10** (Fig. 3A). Finally, we found that the tetra-deuterated probe **5**-d_4 showed the same SOCE modulation activity as the non-deuterated probe **5** (Fig. 3B).

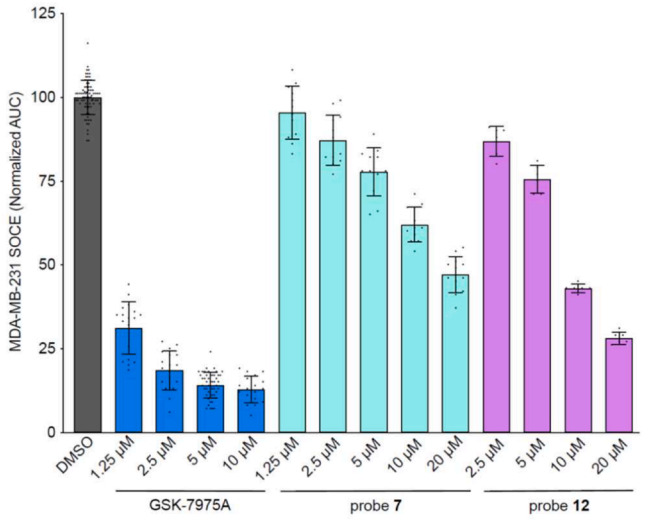

Fig. 2. Modulation of SOCE by bifunctionalised GSK-7975A probe **7** and its inverted congener **12** measured by FLIPR assay. Quantification of Ca^{2+} influx into MDA-MB-231 cells after $CaCl_2$ application (area under the curve (AUC)) in the presence of GSK-7975A, **7** or **12**, normalised to negative control (0.1 % DMSO). Data shown are mean ± SD. The data for GSK-7975A and probe **7**, displayed here, is reiterated from Fig. 1 for direct comparison with inverted probe **12**.

2.3. Evaluation of photo-activatable GSK-7975A probes

2.3.1. Optimisation of irradiation conditions

In order to find the optimal conditions for the photo-decaging (with probe **23**) and photo-crosslinking experiments (with probes **5–9** and **12**) we first conducted a control experiment with the cells alone. HEK293 cells overexpressing human Orai1 (hOrai1) were irradiated for 10 min with 302 nm or 365 nm UV light using a commercially available UV lamp (8 W). Tetrafluorophenyl azide crosslinkers (**6, 8, 9**) are usually photo-activated at 302 nm, whereas phenyldiazirines (**5, 7, 12**) can be photo-activated at longer wavelengths (365 nm). Analysis by Western blot showed that irradiation at the higher energy wavelength (302 nm) caused aggregation of hOrai1 proteins and generation of a broad band at high molecular weight of 250 kDa (Figure S3). In contrary, using the far-UV wavelength at 365 nm did not lead to hOrai aggregation, compared to non-irradiated control.

We then studied the kinetics of photo-fragmentation with 365 nm light of our photo-crosslinking probes in DMSO-d_6 solvent and followed the progress of the photo-reactions by ^{19}F NMR (Figure S4). The model reaction with tetrafluorophenyl azide **9** showed very slow activation and even after 30 min irradiation mainly starting azide **9** was left (Figure S4B). Conversely, activation of diazirine **7** at 365 nm was much faster and after 15 min approximately 70 % of **7** was converted (Figure S4C).

We felt that the photo-activation of diazirines was still on a long time scale, which might bear the risk of damaging biological material. The commercially available UV lamp uses a cylindrical light tube and emits photons in all directions (360°). Taking inspiration from a photo-crosslinking study that used a custom-build UV LED lamp [43] we decided to build our own LED irradiation device (Figure S5). LED light typically allows emission at smaller angles and can be focussed by a condenser lens (Figure S5A) to result in higher irradiation intensity on a defined area (*e.g.* one well in a 6-well cell culture plate, Figure S5B). Furthermore, we also attached a heat sink (Figure S5A) to prevent warming of the sample. This custom-build UV LED lamp was tested in a model experiment with **7** in DMSO-d_6 solution. Strikingly, we recorded an 82 % conversion of **7** by NMR after only 30 s of irradiation at 365 nm (Figure S6), which is approximately 45-times faster than with the previous commercial 8W-UV lamp.

2.3.2. Evaluation of photo-caged GSK-7975A probe

Taking inspiration from the experimental outcome that a large group on the phenolic position of GSK-7975A completely diminished SOCE inhibitory activity (probe **14**, Fig. 3A), we blocked the very same position with a bulky photo-cleavable group (caged probe **23**, Scheme S6) in order to switch off its SOCE activity. The photo-decaging reaction of masked probe **23** with near-UV light is shown in Scheme S7. The indicated allylic bond fragments homolytically and subsequent decarboxylation yields the active GSK-7975A and coumarin blocking group **20**. In a proof-of-concept experiment, a solution of **23** was divided in half, whereas one aliquot was irradiated with 365 nm light for 20 s (using the new UV LED lamp, see 2.3.1) and the other aliquot kept in the dark. Both samples were analysed by HPLC and LC-MS showing that 55 % GSK-7975A was produced after 20 s irradiation (Figure S7). The activity of photo-decaged **23** on I_{CRAC} was investigated in a patch-clamp electrophysiology experiment (Fig. 4). We took HEK293 cells that stably express STIM1 and transfected them with GFP-hOrai1. I_{CRAC} was activated with 50 μM inositol trisphosphate (IP_3) and 20 mM BAPTA. Whilst application of GSK-7975A solution (20 μM) gave a complete block of I_{CRAC}, control experiments with the same concentration of DMSO or non-irradiated **23** did not inhibit I_{CRAC} (Fig. 4). Conversely, an irradiated sample of **23** (20 μM, 365 nm, 20 s) produced 53 % block of I_{CRAC}, which corresponds to the GSK-7975A produced under these irradiation conditions (Figure S7B). Furthermore, we also observed some small I_{CRAC} inhibition with the coumarin masking group **20**. The patch-clamp experiments show that caged **23** is inactive and can efficiently and rapidly

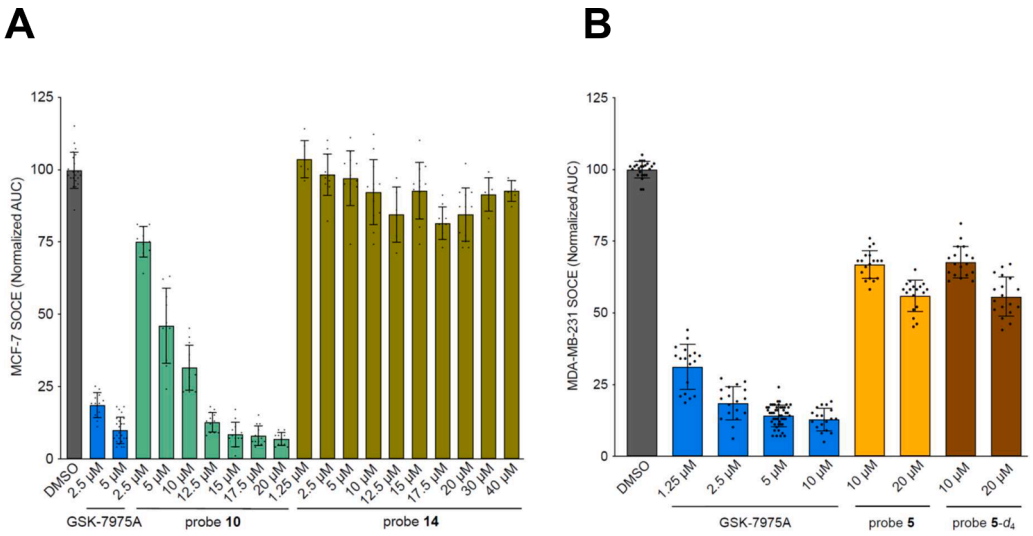

Fig. 3. (**A**) Modulation of SOCE by biotinylated GSK-7975A probe **14** and (**B**) deuterated photo-crosslinking probe **5**-d_4 measured by FLIPR assay. Quantification of Ca^{2+} influx into MCF-7 or MDA-MB-231 cells after $CaCl_2$ application (area under the curve (AUC)) in the presence of GSK-7975A, **10, 14, 5** or **5**-d_4, normalised to negative control (0.1 % DMSO). Data shown are mean ± SD. The data for GSK-7975A and probe **5**, displayed in panel B, is reiterated from Fig. 1 for direct comparison with deuterated probe **5**-d_4.

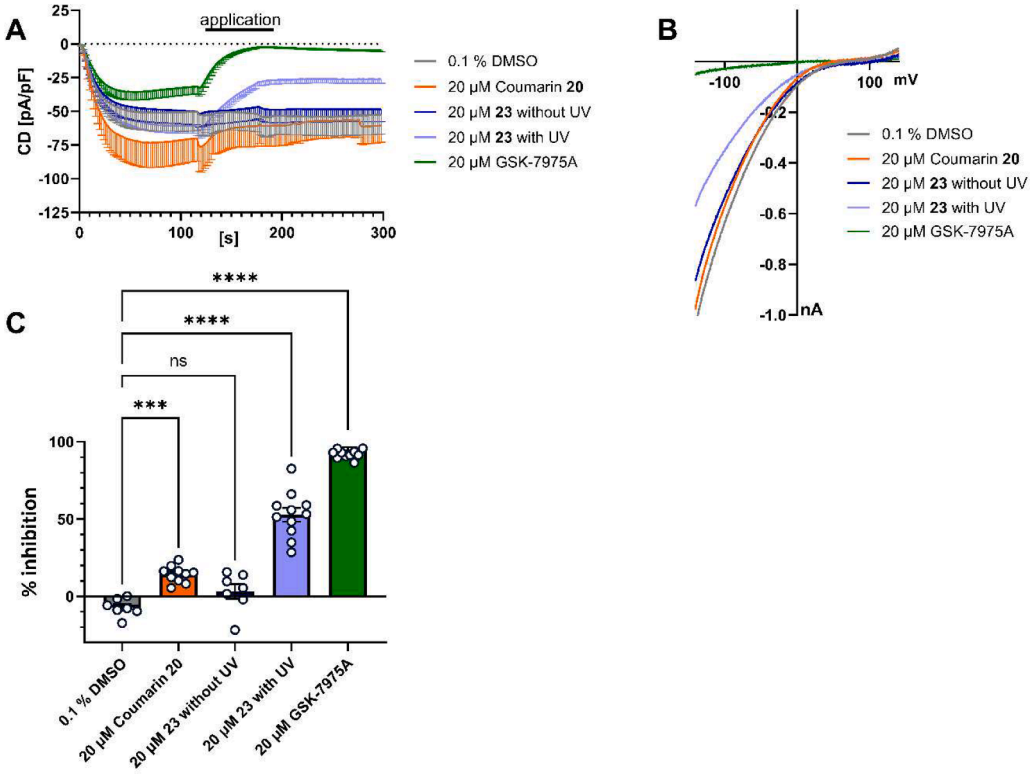

Fig. 4. Effect of coumarin **20**, irradiated or non-irradiated **23** or GSK-7975A on I_{CRAC}. (**A**) I_{CRAC} in HEK293 cells stably overexpressing STIM1 and transiently transfected with GFP-hOrai1. Current densities (CD) recorded under the same condition were averaged and plotted *versus* time (0.1 % DMSO $n = 7$, 20 µM coumarin **20** $n = 10$, 20 µM **23** without UV $n = 7$, 20 µM **23** with UV $n = 11$, 20 µM GSK-7975A $n = 14$). Coumarin **20**, irradiated (365 nm, 20 s) or non-irradiated **23** or GSK-7975A were applied as indicated at concentrations of 20 µM (120 s–180 s). 0.1 % DMSO was used as control. (**B**) Corresponding IV relationship curves at 178 s (end of application) from cells analysed in (**A**). (**C**) Average inhibition of I_{CRAC} as ratio of CD at 178 s (end of application) and CD at 116 s (before application) in percent under the conditions in (**A**) and (**B**) (statistical significance determined by one-way ANOVA, Dunnett's multiple comparison test).

release active SOCE inhibitor GSK-7975A upon irradiation using the UV LED lamp. It is worth to mention that such coumarin cages can also be cleaved using 2-photon excitation (using 750–800 nm light) [44]. Such low energy near-IR light would cause less cell and tissue damage and allow deeper tissue penetration, thus making **23** a promising probe for spatially and temporally resolved *in vitro* and *in vivo* SOCE modulation studies.

2.3.3. *Evaluation of photo-crosslinking probes on hOrai1*

A few years ago, Gill and co-workers reported that mutating four

amino acids in the STIM1-binding nexus region of hOrai1 (L261A, V262N, H264G and K265A, termed hOrai1-ANSGA) leads to constitutively active Orai1 channels independent of STIM1 gating [45]. In a recent study, we have shown that the Orai-ANSGA mutant conveys constitutive activity to human and Xenopus Orai1, but not human Orai2, Orai3 and Drosophila Orai [46]. In addition, we have found that SOCE blockers GSK-7975A and 2-APB efficiently inhibit constitutive activity of hOrai1-ANSGA (Fig. 5).

We therefore considered hOrai1-ANSGA to be a suitable protein model for photo-crosslinking studies of activated hOrai1 at the plasma membrane with our GSK-7975A-derived probes.

In the event, HEK293 cells overexpressing GFP-hOrai-ANSGA were incubated with 40 μM bifunctionalised probe **7** and irradiated with 365 nm light. The membrane fraction was isolated by ultra-centrifugation after mechanical cell lysis and divided equally. One membrane fraction aliquot was treated with biotin-PEG_{11}-azide under CuAAC ("click chemistry") conditions. GFP-fusion proteins were pulled down using GFP-binder beads, separated by SDS PAGE and analysed by Western blot (Fig. 6, lanes 1 and 4). In an alternative workflow, the other membrane fraction aliquot was first affinity-purified with GFP-binder beads and then "clicked" with biotin azide under CuAAC conditions on the resin (Fig. 6, lanes 2 and 5). The band for GFP-hOrai1-ANSGA (calculated 61 kDa) was detected in all samples when probing the Western blot of photo-crosslinking and control experiments (Table 2) with α-GFP antibody (Fig. 6), albeit with different intensities. Whilst the 61 kDa-signal was clearly visible for experiments where the click reaction was performed before GFP-pulldown (lanes 1 and 4), it was strongly diminished for experiments where the click reaction was conducted on the GFP-binder beads after pulldown (lanes 2 and 5). It appears that the added Cu(II)-catalyst is responsible for this effect (compare 61 kDa-bands in lane 2 and 3) and therefore we prefer the first workflow for the photo-crosslinking protein analysis.

Probing the Western blot with horseradish peroxidase-conjugated avidin (avidin-HRP) to detect biotinylated proteins showed fuzzy enrichment of the 61 kDa-band in the sample from experiment 1 (Table 2), indicating photo-crosslink of GFP-hOrai-ANSGA with probe **7** and subsequent click conjugation with the biotin tag. However, we also observed a lot of unspecific bands in this analysis. To check the

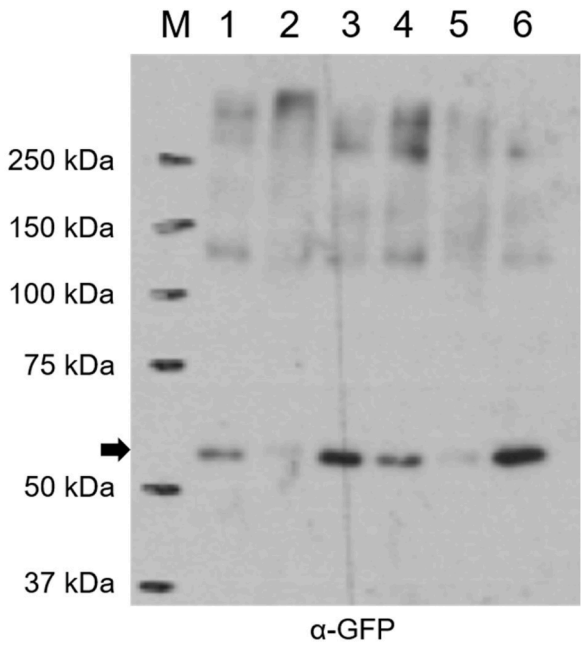

Fig. 6. Western blot analysis of photo-crosslinking and control experiments (Table 2). Blot probed with α-GFP antibody. Black arrow indicates molecular weight of GFP-hOrai1-ANSGA (calculated 61 kDa). M, Marker.

Table 2
Photo-crosslinking (1, 2) and control experiment (3–6) setups.

Experiment/Lane	1	2	3	4	5	6
GFP-hOrai1-ANSGA	+	+	+	+	+	+
probe **7** (40 μM)	+	+	+	–	–	–
CuAAC on membrane fraction	+	–	–	+	–	–
CuAAC on beads	–	+	–	–	+	–
CuAAC on beads without Cu(II)	–	–	+	–	–	–

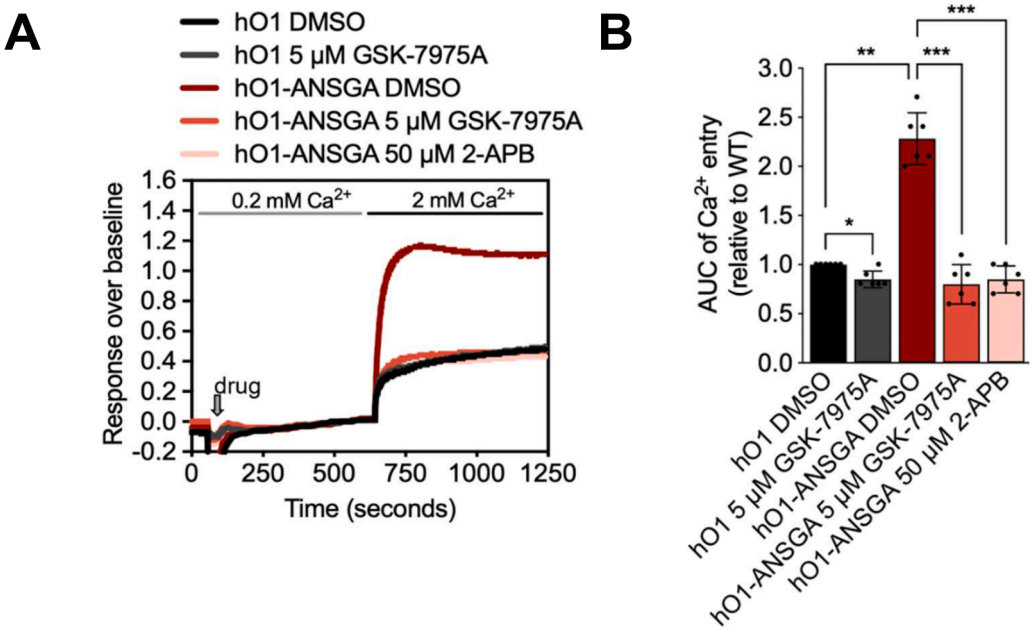

Fig. 5. Blocking of constitutive activity of hOrai1-ANSGA with GSK-7975A and 2-APB. (**A**) Calcium entry measured by FLIPR into HEK293 STIM1/STIM2 double knock-out cells [46] expressing either hOrai1 or hOrai1-ANSGA in the presence of SOCE blockers or DMSO. (**B**) Quantification of Ca^{2+} influx from (**A**) after $CaCl_2$ application (area under the curve (AUC)) relative to hOrai1 WT. Data shown are mean ± SD.

efficiency of the biotinylation via click chemistry, we reacted probe **7** and biotin-PEG_{11}-azide under CuAAC conditions using the membrane fraction resuspension buffer as solvent. According to LC-MS this yielded 59 % desired conjugation product after one hour at room temperature. Although we could obtain some evidence for successful photo-crosslink of GFP-hOrai1-ANSGA with probe **7**, we need to further optimise our protein analysis to be able to reach a final conclusion.

As an alternative approach to directly detect probe photo-crosslink with hOrai1 we also employed protein mass spectrometry (MS) methods. Firstly, we studied the fragmentation pattern of photo-crosslinking probes **5** and **5**-d_4 alone by MS/MS. Both probes were ionised by electrospray (ESI) in MS1 and fragmented similarly by higher energy induced collisional dissociation (HCD) in MS2 (Figure S8). While fragments B_1 and B_2 would correspond to photo-crosslinked peptide adducts, fragment A would provide further evidence for the presence of the probes. These fragmentation patterns were then utilised in the modification site identification analysis. Secondly, we established a suitable protocol for purification and digestion of the target proteins to be analysed by protein MS. HEK293 cells overexpressing either GFP-hOrai1 or GFP-hOrai1-ANSGA were lysed, the target proteins enriched using GFP-binder beads and further purified by SDS-PAGE. The bands with the corresponding mass were cut out and in-gel digested with either trypsin, proteinase K, endoproteinase Glu-C or thermolysin. Analysis of the reaction samples by LC-MS/MS demonstrated that proteinase K digestion (50 °C, 30 min) yielded the highest sequence coverage of 68 % and 67 % for GFP-Orai1 and GFP-Orai1-ANSGA, respectively. Strikingly, the cytosolic and extracellular loops of Orai1 were covered to a great extent, whereas the lipophilic transmembrane domains were hardly detected (Fig. 7), as is often the case for membrane proteins [47].

We performed two separate photo-crosslinking/protein MS experiments using HEK293 cells either overexpressing GFP-hOrai1 or GFP-hOrai1-ANSGA. In one experiment, the cells were incubated with a 1:1-mixture of **5** and **5**-d_4 and in the other they were incubated with only **5**. The mixtures were irradiated with 365 nm light and the cells were processed as described above (cell lysis, GFP-binder beads affinity purification, SDS-PAGE, proteinase K digestion of cut out gel bands). Digestion samples were injected into the mass spectrometer and the data analysed using Proteome Discoverer and MaxQuant software. Despite several searches and simulations, including all amino acids and possible isotope patterns (for mixed isotope experiments with **5** and **5**-d_4), we were unable to detect modified Orai1 peptide fragments in MS/MS spectra that would support successful photo-crosslink with the probes.

In order to explore potential binding site of GSK-7975A on hOrai1 and plan further experiments, we resorted to molecular modelling. A homology model of hOrai1 [46], derived from the crystal structure of hexameric Orai from Drosophila melanogaster (PDB ID: 4HKR) [48], was used as a template for docking experiments (AutoDock Vina v1.1.2) with the previously solved crystal structure of GSK-7975A [16]. This docking exercise predicted two potential binding locations of GSK-7975A in hOrai1, (i) within extracellular loops between hOrai1 subunits and (ii) in the pore of the channel (Fig. 8A). The predicted binding pose in the pore places the 2,6-difluorophenyl ring of GSK-7975A close to aromatic residues W76 and Y80 (Fig. 8B).

To probe the docking-predicted pore-binding site of GSK-7975A, we generated hOrai1 W76E and Y80E mutants and performed patch-clamp electrophysiology experiments with HEK293 cells overexpressing either wild type or mutant hOrai1 (Fig. 9). We observed that the Y80E mutant gave a higher current than wild type or the W76E construct (Fig. 9A and B). However, regarding inhibition of I_{CRAC} with GSK-7975A, there was no significant difference between wild type hOrai1 and the W76E or Y80E mutants (Fig. 9C and D). These data therefore did not support interaction of GSK-7975A with residues W76 or Y80 and consequently the pore binding site of GSK-7975A predicted from the docking experiment.

3. Conclusions

We synthesised several mono- and bifunctionalised probes based on the known SOCE inhibitor GSK-7975A. Most of these compounds retained their inhibitory activity, which highlights the scope of tolerant modifications of the parent ligand scaffold. Attaching bulky, polar tags like biotin (probe **14**), however, led to total loss of inhibitory activity. Exploiting this experimental finding, we blocked the activity of GSK-7975A by attaching a bulky photo-cleavable protecting group and demonstrated in a cell-based system that probe **23** can be efficiently photo-uncaged and inhibitory activity restored. Caged GSK-7975A probe **23** therefore represents an interesting molecular tool to modulate SOCE in a temporal and spatial fashion in cellular systems. Several photo-crosslinking GSK-7975A probes were also synthesised (**5**–**9** and **12**) and an efficient synthetic route to access tetradeuterated diazirinylbenzoic acid **15** established. The latter compound constitutes a general and useful building block to generate photo-crosslinking probes (*e.g.* **5**-d_4) for target identification and proteomic studies using the mixed isotope strategy. Photo-fragmentation of our probes was optimised by choice of photo-crosslinking moiety and by constructing our own LED irradiation device. We found some evidence for successful photo-crosslink of probe **7** with hOrai1. Nevertheless, we were unable to identify the exact binding site of GSK-7579A in hOrai1 using a combination of our photo-crosslinking probes, protein mass spectrometry, docking and mutagenesis studies. Our future efforts to enhance the

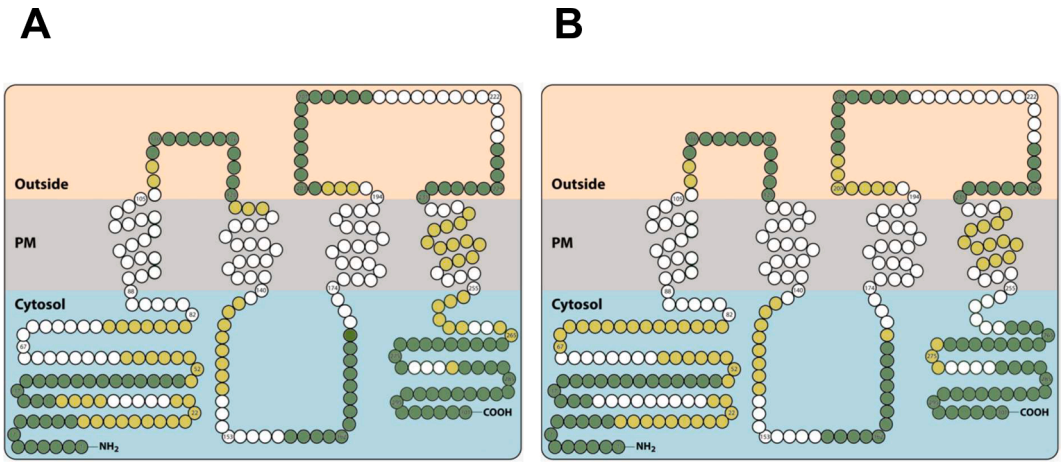

Fig. 7. Snake plot of protein sequence coverage after proteinase K digestion and analysis by LC-MS/MS of (**A**) GFP-hOrai1 and (**B**) GFP-hOrai1-ANSGA. GFP sequence was omitted for clarity. High confidence in dark green, medium confidence in light green, no coverage in white. PM, plasma membrane.

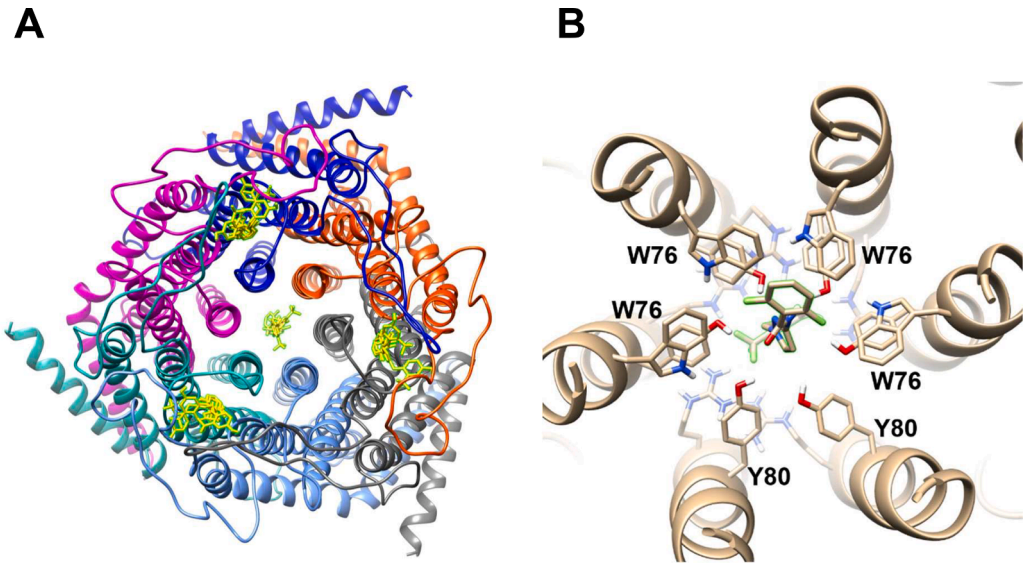

Fig. 8. Docking of GSK-7975A into a hOrai1 homology model. (**A**) Extracellular view of hOrai1 model with docked GSK-7975A poses as yellows sticks, indicating predicted binding sites within the intracellular loops between subunits and in the pore. (**B**) Intracellular view of predicted pore binding site. Potential interaction of docked GSK-7975A (green outline) with aromatic residues W76 and Y80. Two W76 residues have been omitted to show the Y80 residues more clearly.

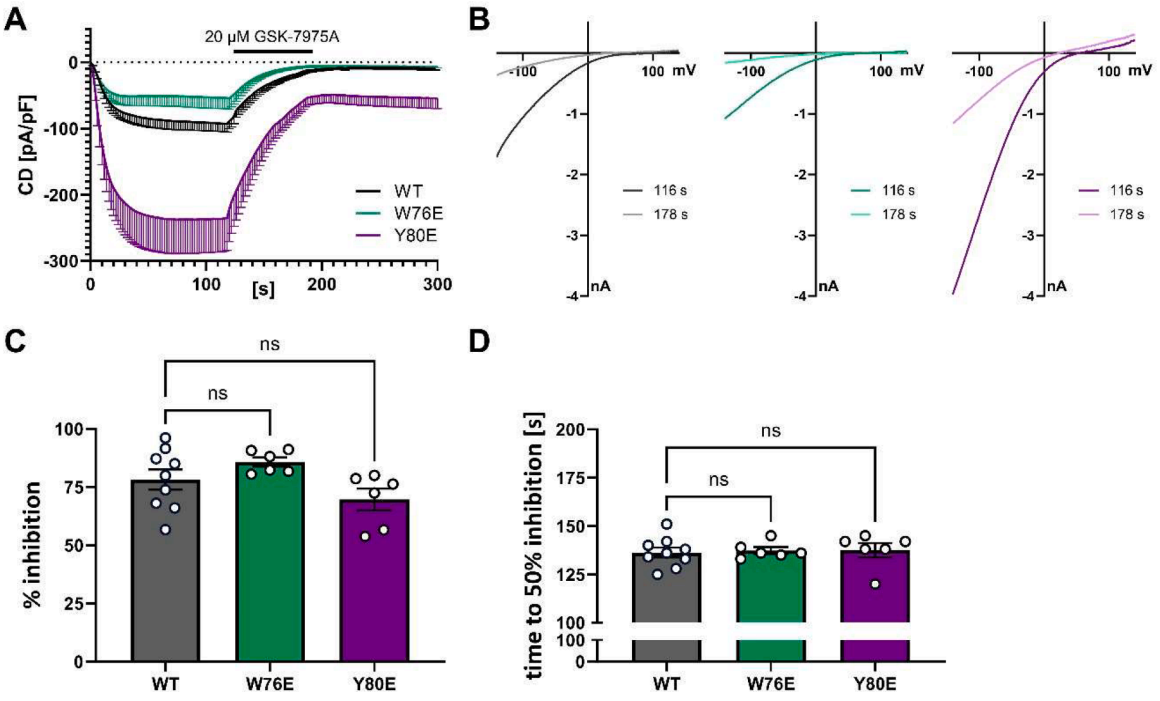

Fig. 9. Inhibition of I_{CRAC} with GSK-7975A when hOrai1 WT or hOrai1 mutants are expressed. (**A**) I_{CRAC} in HEK293 cells stably overexpressing STIM1 with transient overexpression of either hOrai1 WT ($n = 9$), W76E ($n = 6$) or Y80E ($n = 6$). 20 µM GSK-7975A was applied as indicated (black bar, between 120 s and 180 s). (**B**) Corresponding IV relationship curves at either 116 s (before application) or 178 s (end of application) for hOrai1 WT (grey), W79E (green) or Y80E (purple). (**C**) Average inhibition of I_{CRAC} as ratio of current density (CD) at 178 s (end of application) and CD at 116 s (before application) in percent under the conditions in (**A**) and (**B**). (**D**) Average time in seconds, needed to reach 50 % of the current inhibition. Statistical significance determined by one-way ANOVA, Dunnett's multiple comparison test.

depth of coverage of Orai1 residues using mass spectrometry will be valuable in identifying the binding site of GSK-7579A on Orai1. In conclusion, our GSK-7975A analogues serve as an important toolkit for studying the pharmacological modulation of SOCE, and they pave the way for further derivatisation.

4. Methods

4.1. Chemical synthesis

General remarks: Reagents and solvents were purchased from Sigma-Aldrich, AlfaAesar, TCI Europe, Acros Organics or Fluorochem and were used without further purification or drying. Flash column chromatography was performed on a TeledyneISCO CombiFlash Rf+ machine on

RediSepRf prepacked silica gel columns with cyclohexane (solvent A) and EtOAc (solvent B) as eluents unless otherwise noted. ^{1}H, ^{2}H, ^{13}C and ^{19}F NMR spectra were recorded at 300 or 400 MHz, 61 MHz, 75 or 100 MHz and 282 MHz respectively, on a Bruker Avance 300 and Avance II 400. Chemical shifts (δ) are given in parts per million referenced to TMS ($\delta = 0.00$ ppm ^{1}H-, ^{13}C NMR). Coupling constants J are given in Hertz (Hz). Peak multiplicity are defined as follows: s = singlet, d = doublet, t = triplet, q = quartet, m = multiplet, br = broad, dm = doublet of multiplets. Mass spectra and high resolution mass spectra (HRMS) were recorded on a ThermoScientific LTQ Orbitrap XL spectrometer consisting of a linear ion trap (LTQ) featuring a HCD collision cell, coupled to the Orbitrap mass analyser, equipped with a nanoelectrospray ion source (NSI). MS and HRMS spectra were determined by the Mass Spectrometry Group at the Department of Chemistry, Biochemistry and Pharmaceutical Sciences, University of Bern (Prof. Dr. S. Schürch). The purity of the compounds was determined by UPLC-MS on a Dionex Ultimate 3000 using a reversed-phase column Dionex Acclain RSLC, 120C_{18}, 3 × 50 mm, 2.2 μm, 120 Å pore size, flow 1.2 mL/min. Following gradients were used: 100 % A–100 % D over 7 min (A = 100 % H_2O with 0.1 % TFA, D = H_2O/MeCN 10:90 with 0.1 % TFA). Purity was determined by total absorbance at 254 nm. Final compounds were >96 % pure, except **8**, which was 91 % pure by UPLC. All reactions were performed under inert gas atmosphere by using Schlenk technique.

3-Nitro-1*H*-pyrazole. 1*H*-pyrazol-3-amine (183 mg, 2.2 mmol) was dissolved in water (15 mL) and the solution heated at 40 °C. Subsequently, Oxone (3.39 g, 5.5 mmol) was added in small portions and the suspension stirred overnight. The mixture was allowed to reach room temperature, followed by dilution with sat. aq. $NaHCO_3$. The solution was extracted with Et_2O (3x), and the organic phases were combined, washed with brine, dried over Na_2SO_4, filtered and concentrated under vacuum. The residue was further purified by column chromatography (gradient: 100 % A to A/B 55:45) and yielded the title compound as a white solid (129 mg, 52 %). ^{1}H NMR (300 MHz, DMSO-d_6) δ 13.95 (s, 1H), 8.04 (d, J = 2.6, 1H), 7.04 (d, J = 2.5, 1H). ^{13}C NMR (101 MHz, DMSO-d_6) δ 132.3, 101.8. Quaternary carbon could not be detected. HRMS m/z calculated for $C_3H_4N_3O_2$ $[M + H]^+$: 114.0298; Found: 114.0296.

1-(4-Methoxy-2-(trifluoromethyl)benzyl)-3-nitro-1*H*-pyrazole (2). 3-Nitro-1*H*-pyrazole (571 mg, 5.1 mmol) was dissolved in DMF (20 mL). *i*-Pr_2EtN (0.83 mL, 4.9 mmol) diluted with DMF (2 mL), was added and the reaction mixture stirred for 10 min. 4-methoxy-2-(trifluoromethyl)benzyl bromide (1.26 g, 4.6 mmol) was added and the reaction mixture was stirred at room temperature for 1 h. After completion of the reaction as monitored by TLC, the mixture was taken up in water and EtOAc, the layers were separated and the aqueous layer extracted with EtOAc (3x). The combined organic phases were washed with brine, dried over Na_2SO_4, filtered and the solvent was evaporated. Purification was done by column chromatography (gradient: 100 % A to A/B 85:15) and gave product **2** as white solid (1.257 g, 91 %). ^{1}H NMR (300 MHz, Methanol-d_4) δ 7.73 (d, J = 2.5, 1H), 7.31 (d, J = 8.6, 1H), 7.27 (d, J = 2.6, 1H), 7.19 (dd, J = 8.6, 2.6, 1H), 6.96 (d, J = 2.6, 1H), 5.54 (s, 2H), 3.86 (s, 3H). ^{13}C NMR (101 MHz, Methanol-d_4) δ 161.3, 157.3, 134.6, 134.1, 130.5 (q, J = 30.8), 125.6 (q, J = 1.4), 125.4 (q, J = 273.3), 118.4 (q, J = 0.6), 113.6 (q, J = 5.8), 103.8, 56.2, 54.2 (q, J = 2.3). ^{19}F NMR (282 MHz, Methanol-d_4) δ −61.06 (s). HRMS m/z calculated for $C_{12}H_{11}F_3N_3O_3$ $[M + H]^+$: 302.0747; Found: 302.0743.

4-((3-Nitro-1*H*-pyrazol-1-yl)methyl)-3-(trifluoromethyl)phenol (1). To a solution of the aryl methyl ether **2** (1 g, 3.34 mmol) was added magnesium iodide (1.93 g, 6.94 mmol) and [bmim]BF_4 (5 mL). The reaction mixture was heated to 50 °C and stirred for 3 days. As TLC showed no further progress, the mixture was quenched with 5 % aq. $Na_2S_2O_3$ solution (80 mL), the product extracted with EtOAc (3x) and the combined organic layers washed with brine, dried over Na_2SO_4 and filtered. The solvent was removed *in vacuo* and the crude mixture purified by column chromatography (gradient: 100 % A to A/B 70:30) to give the desired phenolic product **1** (white solid, 548 mg, 57 %, 65 % brsm). ^{1}H NMR (300 MHz, Methanol-d_4) δ 7.68 (d, J = 2.5, 1H), 7.23 (d, J = 8.4, 1H), 7.14 (d, J = 2.6, 1H), 7.02 (dd, J = 8.4, 2.5, 1H), 6.95 (d, J = 2.6, 1H), 5.50 (s, 2H). ^{13}C NMR (101 MHz, Methanol-d_4) δ 158.1, 155.8, 133.0, 132.8, 129.2 (q, J = 30.6), 124.1 (q, J = 273.2), 122.6 (q, J = 1.5), 118.8, 112.9 (q, J = 5.8), 102.3, 52.9 (q, J = 2.4). ^{19}F NMR (282 MHz, Methanol-d_4) δ −61.09 (s). HRMS m/z calculated for $C_{11}H_9F_3N_3O_3$ $[M + H]^+$: 288.0591; Found: 288.0604.

3-Nitro-1-(4-(prop-2-yn-1-yloxy)-2-(trifluoromethyl)benzyl)-1*H*-pyrazole (3b). Phenol **1** (102 mg, 0.354 mmol) and Cs_2CO_3 (143 mg, 0.439 mmol) were weighed into a 10 mL round-bottom flask and put under argon. DMF (0.5 mL) was added and the mixture stirred for 15 min at room temperature. Subsequently, propargyl bromide (71 mg, 0.479 mmol) dissolved in DMF (0.5 mL) was added and stirring at room temperature was continued for 1 h. As TLC control indicated completion, EtOAc and brine were added, the layers separated and the aqueous phase extracted with EtOAc (2x). The combined organic phases were washed with brine, dried over Na_2SO_4, filtered and the solvent was evaporated under reduced pressure to give pure **3b** as a white solid in quantitative yield (115 mg). ^{1}H NMR (300 MHz, Methanol-d_4) δ 7.77 (d, J = 2.5, 1H), 7.37 (d, J = 2.4, 1H), 7.33 (d, J = 8.6, 1H), 7.28 (dd, J = 8.6, 2.5, 1H), 6.98 (d, J = 2.6, 1H), 5.58 (s, 2H), 4.85 (d, J = 2.4, 2H), 3.03 (t, J = 2.4, 1H). ^{13}C NMR (101 MHz, Methanol-d_4) δ 159.2, 157.3, 134.7, 133.9, 130.4 (q, J = 31.0), 126.5 (q, J = 1.4), 125.3 (q, J = 273.4), 119.6, 114.6 (q, J = 5.8), 103.8, 78.9, 77.7, 57.1, 54.1 (q, J = 2.4). ^{19}F NMR (282 MHz, Methanol-d_4) δ −61.09 (s). HRMS m/z calculated for $C_{14}H_{11}F_3N_3O_3$ $[M + H]^+$: 326.0747; Found: 326.0745.

1-(4-((3-Nitro-1*H*-pyrazol-1-yl)methyl)-3-(trifluoromethyl)phenoxy)propan-2-one (3c). Phenol **1** (57 mg, 0.197 mmol) and Cs_2CO_3 (173 mg, 0.530 mmol) were dissolved in dry DMF (0.5 mL). After stirring for 30 min, 1-chloropropan-2-one (121 mg, 105 μL, 0.985 mmol) in DMF (0.5 mL) was added and the mixture stirred at ambient temperature. The reaction was monitored by TLC and after completion (2 h), the solution was diluted with brine and EtOAc and the layers separated. The aqueous phase was extracted with EtOAc (2x) and the combined organic layers were washed with brine (3x), dried over Na_2SO_4 and filtered. The solvent was evaporated and the crude purified by column chromatography (gradient: 100 % A to A/B 60:40) providing **3c** as white solid (66 mg, 97 %). ^{1}H NMR (300 MHz, DMSO-d_6) δ 8.09 (d, J = 2.5, 1H), 7.29 – 7.20 (m, 3H), 7.09 (d, J = 2.5, 1H), 5.57 (s, 2H), 4.97 (s, 2H), 2.15 (s, 3H). ^{13}C NMR (101 MHz, Methanol-d_4) δ 205.7, 160.5, 159.6, 134.7, 134.0, 130.6 (q, J = 30.1), 126.6 – 126.5 (m), 125.3 (q, J = 273.5), 119.1, 114.5 (q, J = 5.9), 73.8, 54.1 (q, J = 2.4), 26.2. ^{19}F NMR (282 MHz, DMSO-d_6) δ −58.44 (s). HRMS m/z calculated for $C_{14}H_{13}F_3N_3O_4$ $[M + H]^+$: 344.0853; Found: 344.0860.

4-((3-Amino-1*H*-pyrazol-1-yl)methyl)-3-(trifluoromethyl) phenol (4a). Phenol **1** (173 mg, 0.602 mmol) was dissolved in ethanol (10 mL) and $SnCl_2$ (952 mg, 3.01 mmol) was added. The resulting mixture was heated at reflux for 4 h until TLC showed completion of the reaction. The heating was stopped and the reaction mixture poured into a beaker with ice-cold water (20 mL). Then, 20 % aq. NaOH solution was added (20 mL) and the solution filtered through celite. The filtrate was adjusted to pH 7 by adding 10 % aq. HCl. EtOAc was added, the layers separated and the aqueous phase extracted with EtOAc (2x). The combined organic layers were dried over Na_2SO_4, filtered and the solvents evaporated. Purification by silica column chromatography (gradient: 100 % A–100 % B) afforded title compound **4a** as a white solid (120 mg, 78 %). ^{1}H NMR (300 MHz, DMSO-d_6) δ 10.06 (s, 1H), 7.37 (d, J = 2.3, 1H), 7.06 (d, J = 2.5, 1H), 6.97 (dd, J = 8.5, 2.5, 1H), 6.84 (d, J = 8.5, 1H), 5.43 (d, J = 2.3, 1H), 5.09 (s, 2H), 4.60 (s, 2H). ^{13}C NMR (101 MHz, DMSO-d_6) δ 156.6, 155.8, 131.3, 131.2, 126.9 (q, J = 30.0), 126.3 – 126.1 (m), 128.3 – 119.9 (m), 119.1, 112.2 (q, J = 5.7), 92.3, 50.2 (q, J = 2.8). ^{19}F NMR (282 MHz, DMSO-d_6) δ −58.64 (s). HRMS m/z calculated for $C_{11}H_{11}F_3N_3O$ $[M + H]^+$: 258.0849; Found: 258.0848.

1-(4-(Prop-2-yn-1-yloxy)-2-(trifluoromethyl)benzyl)−1*H*-pyrazol-3-amine (4b). To an ice-cold solution of **3b** (111 mg, 0.341 mmol) in EtOH (4 mL) $SnCl_2$ (539 mg, 2.84 mmol) was added. The ice-bath was

removed and the reaction stirred for 15 min at room temperature, then heated to reflux. TLC control showed complete conversion after 1.5 h, thus the heating was stopped and reaction allowed to reach room temperature. The excess of $SnCl_2$ was quenched with 2 M aq. NaOH solution, diluted with EtOAc and filtered through a pad of celite. The layers were separated, the aqueous phase extracted with EtOAc (2x) and the combined organic layers washed with brine. The organic phase was further dried over Na_2SO_4, filtered and the solvent evaporated. Drying the product under high vacuum and in a desiccator overnight afforded title compound **4b** as slightly yellowish solid in quantitative yield (101 mg). ^{1}H NMR (300 MHz, DMSO-d_6) δ 7.43 (d, J = 2.3, 1H), 7.28 (d, J = 2.7, 1H), 7.24 (dd, J = 8.6, 2.7, 1H), 6.91 (d, J = 8.6, 1H), 5.45 (d, J = 2.3, 1H), 5.15 (s, 2H), 4.89 (d, J = 2.4, 2H), 4.63 (s, 2H), 3.60 (t, J = 2.4, 1H). ^{13}C NMR (75 MHz, DMSO-d_6) δ 156.1, 156.0, 131.5, 131.0, 129.1 – 129.0 (m), 127.7 – 126.2 (m), 123.9 (q, J = 274.4), 118.9 – 118.8 (m), 112.3 (q, J = 5.6), 92.4, 78.8, 78.6, 55.9, 50.1 (q, J = 2.6). ^{19}F NMR (282 MHz, Methanol-d_4) δ −58.58 (s). HRMS *m/z* calculated for $C_{14}H_{13}F_3N_3O$ $[M + H]^+$: 296.1005; Found: 296.1003.

1-(4-((3-Amino-1*H*-pyrazol-1-yl)methyl)-3-(trifluoromethyl) phenoxy)propan-2-one (4c). To an ice-cold solution of **3c** (56 mg, 0.162 mmol) in EtOH (3 mL) $SnCl_2$ (190 mg, 0.808 mmol) was added and the resulting mixture was heated to reflux. TLC showed completion of the reaction after 3 h. Subsequently, heating was removed and ice-cold water was added to the reaction. The mixture was further diluted with 1 M NaOH and EtOAc followed by filtration through celite. The layers were separated, the aqueous phase extracted with EtOAc (2x) and the combined organic layers dried (Na_2SO_4), filtered and concentrated to receive the crude product as yellowish solid. Product **4c** was immediately used without further purification in the next step. ^{19}F NMR (282 MHz, DMSO-d_6) δ -58.56 (s). HRMS *m/z* calculated for $C_{14}H_{15}F_3N_3O_2$ $[M + H]^+$: 314.1111; Found: 314.1121.

***N*-(1-(4-Hydroxy-2-(trifluoromethyl)benzyl)-1*H*-pyrazol-3-yl)-4-(3-(trifluoromethyl)-3*H*-diazirin-3-yl)benzamide (5).** 4-(3-(Trifluoromethyl)-3*H*-diazirin-3-yl)benzoic acid [47,49] (48 mg, 0.209 mmol) and HATU (72 mg, 0.189 mmol) were dissolved in DMF (1 mL) followed by the addition of *i*-Pr_2EtN (32 μL, 0.186 mmol) in DMF (1 mL). The reaction vessel was wrapped in aluminium foil and the mixture stirred for 15 min at ambient temperature before adding the amine **4a** (44 mg, 0.171 mmol) in DMF (1.5 mL). Stirring overnight at room temperature indicated full consumption of the amine by TLC and the reaction was worked up. The mixture was diluted with brine and EtOAc and the layers were separated. The aqueous layer was extracted with EtOAc (2x) and the combined organic layers were washed with brine, dried over Na_2SO_4 and filtered. The solvent was evaporated under reduced pressure and purification by column chromatography (gradient: 100 % A to A/B 65:35) delivered product **5** as a white solid (62 mg, 78 %). ^{1}H NMR (300 MHz, DMSO-d_6) δ 11.07 (s, 1H), 10.15 (s, 1H), 8.09 (d, J = 8.5, 2H), 7.74 (d, J = 2.3, 1H), 7.37 (d, J = 8.1, 2H), 7.09 (d, J = 2.5, 1H), 7.01 (dd, J = 8.6, 2.5, 1H), 6.91 (d, J = 8.6, 1H), 6.69 (d, J = 2.3, 1H), 5.34 (s, 2H). ^{13}C NMR (101 MHz, Methanol-d_4) δ 166.6, 158.8, 148.6, 137.0, 133.4, 132.9, 132.3, 131.3, 130.5, 130.0, 129.7, 129.4, 127.7 (q, J = 1.6), 126.4 (d, J = 1.4), 125.6 (q, J = 273.4), 123.4 (q, J = 274.0), 123.1, 113.9 (q, J = 5.9), 99.6, 52.6 (q, J = 2.6). ^{19}F NMR (282 MHz, DMSO-d_6) δ−58.65 (s), −64.37 (s). HRMS *m/z* calculated for $C_{20}H_{14}F_6N_5O_2$ $[M + H]^+$: 470.1046; Found: 470.1067.

4-Azido-2,3,5,6-tetrafluoro-*N*-(1-(4-(prop-2-yn-1-yloxy)-2-(trifluoromethyl)benzyl)-1*H*-pyrazol-3-yl)benzamide (6). 4-Azido-2,3,5,6-tetrafluorobenzoic acid [50] (61 mg, 0.259 mmol) was dissolved in DMF (1 mL) followed by the addition of *i*-Pr_2EtN (43 μL, 0.257 mmol) and HATU (98 mg, 0.257 mmol). The reaction vessel was wrapped in aluminium foil and the mixture stirred for 30 min, before adding the amine **4b** (68 mg, 0.230 mmol) in DMF (1.5 mL). After 2 h of stirring at room temperature, TLC indicated complete consumption of the amine and the reaction was worked up. EtOAc and brine were added and the layers separated. The aqueous phase was extracted with EtOAc (3x) and subsequently the combined organic layers washed with brine, dried over Na_2SO_4, filtered and the solvents evaporated *in vacuo*. The crude product was purified by column chromatography (gradient: 100 % A to A/B 70:30) resulting in product **6** as a white solid (93 mg, 78 %). ^{1}H NMR (300 MHz, DMSO-d_6) δ 11.55 (s, 1H), 7.83 (d, J = 2.3, 1H), 7.35 – 7.25 (m, 2H), 7.10 (d, J = 8.5, 1H), 6.64 (d, J = 2.3, 1H), 5.39 (s, 2H), 4.91 (d, J = 2.3, 2H), 3.62 (t, J = 2.3, 1H). ^{13}C NMR (101 MHz, Methanol-d_4) δ 158.6, 157.3 – 157.1 (m), 148.0, 145.2 (d, J = 249.0), 142.0 (dm, J = 249.9), 132.7, 132.5, 129.8 (q, J = 30.9), 128.9 (q, J = 1.4), 125.5 (q, J = 273.4), 123.6 – 123.2 (m), 119.5, 114.2 (q, J = 5.9), 113.1 (t, J = 20.2), 99.3, 79.0, 77.5, 57.0, 52.5 (q, J = 2.9). ^{19}F NMR (282 MHz, DMSO-d_6) δ −135.77 – −144.94 (m), −147.07 – −158.96 (m). HRMS *m/z* calculated for $C_{21}H_{12}F_7N_6O_2$ $[M + H]^+$: 513.0904; Found: 513.0899.

***N*-(1-(4-(Prop-2-yn-1-yloxy)-2-(trifluoromethyl)benzyl)-1*H*-pyrazol-3-yl)-4-(3-(trifluoromethyl)-3*H*-diazirin-3-yl)benzamide (7).** To 4-(3-(Trifluoromethyl)-3*H*-diazirin-3-yl)benzoic acid [47,49] (59 mg, 0.256 mmol) and HATU (98 mg, 0.258 mmol) in DMF (1 mL), *i*-Pr_2EtN (45 μL, 0.263 mmol) in DMF (1 mL) was added. The reaction vessel was wrapped in aluminium foil and the mixture stirred for 15 min at ambient temperature before adding the amine **4b** (71 mg, 0.239 mmol) in DMF (1 mL). Stirring at room temperature overnight led to complete consumption of the amine. The reaction was diluted with brine and EtOAc and the layers were separated. The aqueous layer was extracted with EtOAc (2x). The combined organic layers were washed with brine, dried over Na_2SO_4, filtered and the solvent evaporated under reduced pressure. Column chromatography (gradient: 100 % A to A/B 75:25) provided product **7** as a colourless oil (115 mg, 94 %). ^{1}H NMR (300 MHz, DMSO-d_6) δ 11.07 (s, 1H), 8.09 (d, J = 8.5, 2H), 7.80 (d, J = 2.3, 1H), 7.37 (d, J = 8.2, 2H), 7.33 (d, J = 2.7, 1H), 7.31 – 7.25 (m, 1H), 7.01 (d, J = 8.5, 1H), 6.71 (d, J = 2.3, 1H), 5.40 (s, 2H), 4.91 (d, J = 2.4, 2H), 3.62 (t, J = 2.4, 1H). ^{13}C NMR (101 MHz, Methanol-d_4) δ 166.6, 158.6, 148.8, 137.0, 133.4, 132.6, 132.6, 129.9, 129.6, 129.0 (q, J = 1.4), 127.8 – 127.6 (m), 125.5 (q, J = 273.4), 123.4 (q, J = 273.8), 119.5, 114.2 (q, J = 6.0), 99.7, 79.0, 77.5, 57.0, 52.5 (q, J = 3.0). ^{19}F NMR (282 MHz, DMSO-d_6) δ −58.55 (s), −64.37 (s). HRMS *m/z* calculated for $C_{23}H_{16}F_6N_5O_2$ $[M + H]^+$: 508.1203; Found: 508.1205.

4-Azido-2,3,5,6-tetrafluoro-*N*-(1-(4-(2-oxopropoxy)-2-(trifluoromethyl)benzyl)-1*H*-pyrazol-3-yl)benzamide (8). 4-Azido-2,3,5,6-tetrafluorobenzoic acid [50] (32 mg, 0.137 mmol) was dissolved in DMF (1.5 mL) followed by the addition of *i*-Pr_2EtN (23 μL, 0.137 mmol) and HATU (52 mg, 0.137 mmol). The reaction vessel was wrapped in aluminium foil and the mixture stirred for 15 min at ambient temperature before adding the amine **4c** (39 mg, 0.125 mmol) in DMF (1 mL). TLC monitoring did not show completion, thus stirring was continued overnight followed by a second addition of *i*-Pr_2EtN (23 μL, 0.137 mmol) in DMF (0.5 mL). Since TLC did not show further progress the reaction was worked up after 48 h. The mixture was then neutralised with 1 M HCl and the solvent evaporated in high vacuum. The residue was purified by column chromatography twice (gradient: 100 % A to A/B 30:70) to yield product **8** as a white solid (5 mg, 8 %). ^{1}H NMR (300 MHz, Acetonitrile-d_3) δ 9.26 (s, 1H), 7.54 (d, J = 2.4, 1H), 7.24 (d, J = 2.7, 1H), 7.05 (dd, J = 8.7, 2.7, 1H), 6.97 (d, J = 8.7, 1H), 6.70 (d, J = 2.4, 1H), 5.36 (s, 2H), 4.77 (s, 2H), 2.16 (s, 3H). ^{13}C NMR (101 MHz, Acetonitrile-d_3) δ 204.2, 158.6, 147.4, 132.6, 132.4, 128.7 – 128.4 (m), 119.0, 113.8 (q, J = 5.8), 98.7, 73.6, 52.4 (q, J = 2.6), 30.4, 26.5 (not all carbons detected). ^{19}F NMR (282 MHz, Acetonitrile-d_3) δ −60.36, −141.00 – −145.55 (m), - 149.58 – −152.89 (m). HRMS *m/z* calculated for $C_{21}H_{14}F_7N_6O_3$ $[M + H]^+$: 531.1010; Found: 531.0994.

4-Azido-2,3,5,6-tetrafluoro-*N*-(1-(4-hydroxy-2-(trifluoromethyl)benzyl)-1*H*-pyrazol-3-yl)benzamide (9). 4-Azido-2,3,5,6-tetrafluorobenzoic acid [50] (70.4 mg, 0.299 mmol) was dissolved in DMF (1.5 mL) followed by the addition of *i*-Pr_2EtN (51 μL, 0.299 mmol) and HATU (114 mg, 0.299 mmol). The reaction vessel was wrapped in aluminium foil and the mixture stirred for 15 min at ambient temperature before adding the amine **4a** (70 mg, 0.272 mmol) in DMF (1 mL). The reaction mixture was stirred at room temperature in the

dark for 18 h. TLC showed completion of the reaction and the reaction mixture was diluted with EtOAc (100 mL) and the organic layer washed with 1 M HCl (2 × 100 mL), sat. aq. NaCl (5 × 100 mL) and dried over Na_2SO_4. The solvents were evaporated and the crude product purified by column chromatography (gradient: 100 % A to A/B 75:25) yielding product **9** as a white solid. ^{1}H and ^{13}C NMR spectra were identical to the spectra obtained from the product **9** synthesised by the alternative route (Scheme S2).

2,6-Difluoro-*N*-(1-(4-(prop-2-yn-1-yloxy)-2-(trifluoromethyl) benzyl)-1*H*-pyrazol-3-yl)benzamide (10). 51.0 mg (0.128 mmol) of GSK-7975A (2,6-difluoro-*N*-(1-(4-hydroxy-2-(trifluoromethyl)benzyl)-1*H*-pyrazol-3-yl)benzamide [16]) were dissolved in DMF (2 mL) and propargyl bromide (20.8 mg, 0.14 mmol) was added. After the mixture was cooled to 0 °C, sodium hydride (60 % in mineral oil, 4.9 mg, 0.123 mmol) suspended in DMF (1 mL) was added. Reaction control by TLC indicated completion after two hours. The solvent was evaporated and the residue was taken up in water and DCM. The layers were separated and the aqueous phase extracted with DCM (2x), the combined organic layers were washed with brine, dried over Na_2SO_4, filtered and the solvent was evaporated. Purification by column chromatography (gradient: 100 % A to A/B 70:30) delivered **10** as a white product. (22.6 mg, 41 %). ^{1}H NMR (300 MHz, Methanol-d_4) δ 7.57 (d, J = 2.4, 1H), 7.50 (tt, J = 8.7, 6.4, 1H), 7.32 (d, J = 2.7, 1H), 7.19 (dd, J = 8.7, 2.7, 1H), 7.13 – 6.99 (m, 3H), 6.75 (d, J = 2.4, 1H), 5.41 (s, 2H), 4.80 (d, J = 2.4, 2H), 2.99 (t, J = 2.4, 1H). ^{13}C NMR (75 MHz, Methanol-d_4) δ 161.0 (dd, J = 250.4, 7.2), 160.5, 148.3, 133.3 (t, J = 10.1), 132.6, 132.3, 129.6 (q, J = 31.0), 129.0 – 128.9 (m), 125.4 (q, J = 273.4), 119.5, 115.9 (t, J = 21.7), 114.2 (q, J = 5.9), 113.1 – 112.6 (m), 99.4, 79.0, 77.5, 57.0, 52.4 (q, J = 3.0). ^{19}F NMR (282 MHz, Methanol-d_4) δ −61.27 (s), −115.20 (s). HRMS m/z calculated for $C_{21}H_{15}F_5N_3O_2$ $[M + H]^+$: 436.1079; Found: 436.1073.

2,6-Difluoro-*N*-(1-(4-(2-oxopropoxy)-2-(trifluoromethyl) benzyl)-1*H*-pyrazol-3-yl)benzamide (11). GSK-7975A (2,6-difluoro-*N*-(1-(4-hydroxy-2-(trifluoromethyl)benzyl)-1*H*-pyrazol-3-yl)benzamide [16]) (51.3 mg, 0.132 mmol) was dissolved in DMF (2 mL) and chloroacetone (30.5 mg, 0.329 mmol) was added. After the mixture was cooled to 0 °C, sodium hydride (60 % in mineral oil, 10.5 mg, 0.263 mmol) suspended in DMF was added. The reaction was allowed to reach room temperature overnight. Since TLC control indicated mainly unreacted GSK-7975A, the mixture was heated to 100 °C and another equivalent of chloroacetone (12.2 mg, 0.132 mmol) and 0.5 equivalent of sodium hydride (2.7 mg, 0.07 mmol) was added. After two days with no further progress, the heating was stopped, the solvent evaporated and the residue was taken up in water and DCM. The layers were separated, the aqueous layer extracted with DCM (2x) and the combined organic phases were washed with brine and dried over Na_2SO_4. Filtration and evaporation of the solvent, followed by column chromatography with cyclohexane, EtOAc, aq. ammonia and *i*-Pr_2EtN as eluents (1:1:0.02:0.02) delivered the desired product **11** (20.5 mg, 36 %). ^{1}H NMR (300 MHz, DMSO-d_6) δ 11.29 (s, 1H), 7.79 (d, J = 2.3, 1H), 7.66 – 7.43 (m, 1H), 7.29 – 7.12 (m, 4H), 7.00 (d, J = 8.8, 1H), 6.65 (d, J = 2.3, 1H), 5.37 (s, 2H), 4.94 (s, 2H), 2.15 (s, 3H). ^{13}C NMR (101 MHz, Methanol-d_4) δ 206.0 (t, J = 4.9), 161.1 (dd, J = 250.3, 7.2), 160.5, 159.0, 148.3, 133.3 (t, J = 10.1), 132.5 (d, J = 22.5), 129.8 (q, J = 31.0), 129.0 – 128.9 (m), 125.4 (q, J = 273.4), 119.0, 118.9, 115.9 (t, J = 21.8), 114.1 (q, J = 5.9), 113.1 – 112.6 (m), 99.4, 65.2, 61.5, 52.4 (dd, J = 5.7, 2.8). ^{19}F NMR (282 MHz, DMSO-d_6) δ −58.47, −100.51 – −125.12 (m). HRMS m/z calculated for $C_{21}H_{17}F_5N_3O_3$ $[M + H]^+$: 454.1185; Found: 454.1175.

2,6-Difluoro-*N*-(1-(4-((1-(13-oxo-17-((3a*S*,4*S*,6a*R*)-2-oxohexahydro-1*H*-thieno[3,4-*d*]imidazol-4-yl)-3,6,9-trioxa-12-azaheptadecyl)-1*H*-1,2,3-triazol-4-yl)methoxy)-2-(trifluoromethyl)benzyl)-1*H*-pyrazol-3-yl)benzamide (14). Alkyne **10** (5 mg, 0.011 mmol), TBTA (0.1 mg, $2{\cdot}10^{-4}$ mmol), $CuSO_4{\cdot}5\,H_2O$ (72 μL from an aq. 1 M stock solution, $2{\cdot}10^{-4}$ mmol), Biotin-PEG_3-azide **13** (5.1 mg, 0.011 mmol) and sodium ascorbate (0.7 mg, $3{\cdot}10^{-4}$ mmol) were transferred into a sealed tube, dissolved in a mixture of water and *t*-BuOH (1:1, 1 mL) and stirred at ambient temperature overnight. Without further workup the reaction mixture was submitted to a preparative HPLC on a C18 reverse phase column and the product was eluted with water (acidified with 0.1 % TFA) as solvent A and a mixture of water and MeCN 10:90 (0.1 % TFA) as solvent B running a gradient of 100 % A to 100 % B. Drying of the desired fractions on a lyophilisator afforded click product **14** as a white solid (5.5 mg, 57 %). ^{1}H NMR (300 MHz, DMSO-d_6) δ 11.29 (s, 1H), 8.21 (s, 1H), 7.86 – 7.74 (m, 2H), 7.62 – 7.44 (m, 1H), 7.35 (d, J = 10.6, 2H), 7.17 (t, J = 8.1, 2H), 7.04 (d, J = 8.4, 1H), 6.66 (d, J = 2.3, 1H), 6.38 (d, J = 17.0, 2H), 5.37 (s, 2H), 5.23 (s, 2H), 4.53 (t, J = 5.1, 2H), 4.35 – 4.23 (m, 1H), 4.17 – 4.06 (m, 1H), 3.81 (t, J = 5.1, 2H), 3.72 – 3.44 (m, 4H), 3.36 (t, J = 6.0, 2H), 3.22 – 3.02 (m, 3H), 2.87 – 2.66 (m, 2H), 2.04 (t, J = 7.4, 2H), 1.74 – 1.36 (m, 4H), 1.38 – 1.10 (m, 4H), 0.91 – 0.79 (m, 1H). ^{13}C NMR (101 MHz, DMSO-d_6) δ 172.1, 162.6, 157.6 – 157.3 (m), 146.8, 141.9, 131.7, 131.6, 130.3 – 125.4 (m), 127.1, 125.0, 118.7, 115.2 – 114.7 (m), 112.6 – 112.5 (m), 111.9, 111.8 – 111.6 (m), 97.3, 69.6, 69.6, 69.5, 69.1, 68.6, 61.5, 61.0, 59.2, 55.4, 49.4, 38.4, 35.1, 28.1, 28.0, 25.2. ^{19}F NMR (282 MHz, DMSO-d_6) δ −58.47, −73.69, −113.97. HRMS m/z calculated for $C_{39}H_{47}F_5N_9O_7S$ $[M + H]^+$: 880.3243; Found: 880.3221.

1-Bromo-4-(methyl-d_3)benzene-2,3,5,6-d_4 (16). Powdery NaY type zeolite was heated under high vacuum slowly to 500 °C over two days, then left to cool to room temperature and stored in a glovebox. The zeolite (8.3 g) was transferred into a Schlenk tube and suspended in dry DCM (40 mL) and toluene-d_8 (1.73 mL, 15 mmol). To this solution bromine (0.85 mL, 16.5 mmol) diluted in DCM (5 mL) was added dropwise. The flask was wrapped in aluminium foil and the mixture stirred overnight at ambient temperature. The zeolite was removed by filtration and washed with DCM. The filtrate was treated with sat. aq. $Na_2S_2O_3$ to quench excess bromine and diluted with water. The phases were separated, the aqueous phase extracted with DCM (2x) and the combined organic phases were washed with brine, dried over Na_2SO_4, filtered and the solvent was removed under reduced pressure. The residue was further purified by column chromatography (eluent: 100 % A) affording title compound **16** as a single regioisomer in quantitative yield. ^{2}H NMR (61 MHz, DMSO) δ 7.43 (s, 2D), 7.15 (s, 2D), 2.20 (s, 3D). ^{13}C NMR (101 MHz, DMSO) δ 135.6, 130.3 – 129.1 (m), 117.1, 25.4, 19.3 – 17.5 (m).

2,2,2-Trifluoro-1-(4-(methyl-d_3)phenyl-2,3,5,6-d_4)ethan-1-one (17). Deuterated 4-bromo toluene **16** (1.16 g, 6.51 mmol) was dissolved in THF (20 mL) and cooled to −78 °C, then *n*-BuLi (2.5 M in hexane, 3.13 mL, 7.82 mmol) was slowly added. The mixture was stirred for 30 min at −78 °C before ethyl trifluoroacetate (365 mg, 2.57 mmol) dissolved in THF (5 mL) was added and the reaction stirred for 1.5 h. After completion of the reaction (monitored by TLC) the mixture was allowed to reach room temperature and quenched with sat. aq. NH_4Cl solution. Et_2O was added and the layers were separated. The aqueous layer was extracted with Et_2O (2x) and the combined organic layers were washed with brine, dried over Na_2SO_4, filtered and concentrated carefully under reduced pressure to obtain crude **17** as slightly yellowish oil (1.05 g, 83 %). Further purification by column chromatography on silica gel (gradient: 100 % A to A/B 95:5) provided **17** as colourless oil (826 mg, 65 %). Some product loss can be explained due to azeotropic co-evaporation with solvents under reduced pressure. ^{2}H NMR (61 MHz, DMSO) δ 7.95 (s, 2D), 7.49 (s, 2D), 2.36 (s, 3D). ^{13}C NMR (101 MHz, DMSO) δ 178.32 (q, J = 34.1), 146.3, 129.2 – 127.9 (m), 125.6, 115.5 (q, J = 292.4), 25.4 (d, J = 1.4), 19.5 (dd, J = 38.2, 19.1). ^{19}F NMR (376 MHz, DMSO) δ −69.82.

2,2,2-Trifluoro-1-(4-(methyl-d_3)phenyl-2,3,5,6-d_4)ethan-1-one oxime. To a solution of trifluoroacetate **17** (763 mg, 3.91 mmol) in EtOH (5 mL), hydroxylamine hydrochloride (299 mg, 4.30 mmol) dissolved pyridine (10 mL) was added. The mixture was heated to 80 °C and stirred overnight. As the reaction was completed (indicated by TLC), Et_2O and water were added, the layers separated and the aqueous layer extracted with Et_2O (2x). The collected organic layers were washed with

brine, dried over Na_2SO_4, filtered and the solvent was evaporated under reduced pressure. The residue was purified by column chromatography (gradient: 100 % A to A/B 90:10) to yield the oxime as a mixture of *E* and *Z* isomers (7.78 g, 95 %, *E/Z* 1:0.8, white, crystalline solid). ^{1}H NMR (400 MHz, DMSO-d_6) δ 12.94 (d, J = 1.3, 0.45H), 12.65 (s, 0.55H). ^{2}H NMR (61 MHz, DMSO) δ 7.33 (s, 4D), 2.25 (s, 3D). ^{13}C NMR (101 MHz, DMSO-d_6) δ 145.1 – 144.0 (m), 139.7, 139.4, 129.2 – 127.2 (m), 123.5, 121.2 (q, J = 274.2), 118.5 (q, J = 281.0), 20.7. ^{19}F NMR (282 MHz, DMSO-d_6) δ −61.74, −64.80. HRMS *m/z* calculated for $C_9HD_7F_3NNaO$ $[M+Na]^+$: 233.0890; Found: 233.0896.

2,2,2-Trifluoro-1-(4-(methyl-d_3)phenyl-2,3,5,6-d_4)ethan-1-one *O*-tosyl oxime (18). Oxime from above (734 mg, 3.49 mmol) was dissolved in pyridine (8 mL) at room temperature and *p*-toluenesulfonylchloride (888 mg, 4.66 mmol) was added in small portions. The mixture was stirred for 24 h at 80 °C until TLC showed completion. After cooling to room temperature EtOAc and water were added, the layers separated and the aqueous layer extracted with EtOAc (2x). The combined organic layers were washed with brine, dried over Na_2SO_4, filtered and the solvent was evaporated on a rotary evaporator. Purification by column chromatography (gradient: 100 % A to A/B 90:10) afforded product **18** as a white solid (1.15 mg, 90 %). ^{1}H NMR (400 MHz, DMSO-d_6) δ 7.92 – 7.83 (m, 2H), 7.57 – 7.53 (m, 2H), 2.45 (s, 3H). ^{2}H NMR (61 MHz, DMSO) δ 7.38 (s, 4D), 2.29 (s, 3D). ^{13}C NMR (101 MHz, DMSO-d_6) δ 154.1 (q, J = 33.3, 32.4), 146.7, 142.2, 130.4, 130.2, 129.7 – 128.9 (m), 128.8, 128.2 – 127.4 (m), 120.6, 119.3 (q, J = 277.3), 21.2. ^{19}F NMR (282 MHz, DMSO-d_6) δ −66.05. HRMS *m/z* calculated for $C_{16}H_8D_7F_3NO_3S$ $[M + H]^+$: 365.1159; Found: 365.1153.

3-(4-(Methyl-d_3)phenyl-2,3,5,6-d_4)-3-(trifluoromethyl)diaziridine (19). Tosylated oxime **18** (800 mg, 2.20 mmol) was dissolved in diethyl ether (10 mL) and cooled to −78 °C. The reaction vessel was equipped with a dry ice condenser and ammonia (approx. 15 mL) was condensed into the reaction mixture. The solution was allowed to reach room temperature slowly overnight. The precipitate was removed by filtration and the solution was reduced *in vacuo*. The residue was purified by column chromatography (gradient: 100 % A to A/B 85:15) to give **19** as white solid (440 mg, 96 %). ^{1}H NMR (300 MHz, DMSO-d_6) δ 4.04 (d, J = 8.2, 1H), 3.88 (dd, J = 8.2, 1.7, 1H). ^{2}H NMR (61 MHz, DMSO) δ 7.78 – 6.93 (m, 4D), 2.23 (s, 3D). ^{13}C NMR (101 MHz, DMSO-d_6) δ 138.8, 129.0, 128.8 – 127.5 (m), 124.2 (q, J = 278.6), 57.2 (q, J = 34.8), 20.7. ^{19}F NMR (282 MHz, DMSO-d_6) δ −73.91. HRMS *m/z* calculated for $C_9H_2D_7F_3N_2Na$ $[M+Na]^+$: 232.1049; Found: 232.1047.

4-(3-(Trifluoromethyl)-3*H*-diazirin-3-yl)benzoic-2,3,5,6-d_4 acid (15). To a cooled mixture (17 °C) of diaziridine **19** (40 mg, 0.193 mmol) in glacial acetic acid (2 mL) was slowly added H_2SO_4 (38 µL, 0.717 mmol) while keeping the temperature below 19 °C, followed by the addition of CrO_3 (85 mg, 0.853 mmol) in small portions. Monitoring of the reaction by HPLC showed oxidation of the diaziridine to diazirine within the first 60 min, while the oxidation of the benzylic position required a longer reaction time. The solution was allowed to reach room temperature overnight. A HPLC probe showed completion of the reaction. Water and Et_2O were added and the layers separated. The aqueous layer was extracted with Et_2O (2x) and the combined organic phases were washed with brine, dried over Na_2SO_4, filtered and reduced *in vacuo* to give **15** as a white solid (24 mg, 53 %). ^{1}H NMR (300 MHz, DMSO-d_6) δ 13.29 (s, 1H). ^{2}H NMR (61 MHz, DMSO) δ 8.08 (s, 2D), 7.79 – 7.04 (m, 2D). ^{13}C NMR (101 MHz, DMSO-d_6) δ 66.3, 132.2, 131.7, 130.5 – 129.2 (m), 127.0 – 125.8 (m), 121.7 (q, J = 274.6), 28.0 (q, J = 40.4). ^{19}F NMR (282 MHz, DMSO-d_6) δ −64.38. HRMS *m/z* calculated for $C_9D_4F_3N_2O_2$ $[M-H]^-$: 233.0481; Found: 233.0487.

***N*-(1-(4-Hydroxy-2-(trifluoromethyl)benzyl)-1*H*-pyrazol-3-yl)-4-(3-(trifluoromethyl)-3*H*-diazirin-3-yl)benzamide-2,3,5,6-d_4 (5-d_4).** Carboxylic acid **15** (20 mg, 0.085 mmol) and HATU (35.7 mg, 0.094 mmol) were dissolved in DMF (1 mL) followed by the addition of *i*-Pr_2EtN (16.3 µL, 0.094 mmol) in DMF (1 mL). The reaction vessel was wrapped in aluminium foil and the mixture stirred for 15 min at ambient temperature before adding amine **4a** (33.0 mg, 0.128 mmol) in DMF (1.5 mL). The reaction was stirred overnight at room temperature worked up thereafter by dilution with brine and EtOAc and separation of the layers. The aqueous layer was extracted with EtOAc (2x) and the combined organic phases were washed with brine, dried over Na_2SO_4, filtered and the solvent evaporated under reduced pressure. Column chromatography (gradient: 100 % A to A/B 60:40) delivered final probe **5**-d_4 as a white solid (13.5 mg, 34 %) with tetramethylurea as impurity (11 %). ^{1}H NMR (300 MHz, DMSO-d_6) δ 11.07 (s, 1H), 10.15 (s, 1H), 7.74 (d, J = 2.3, 1H), 7.09 (d, J = 2.5, 1H), 7.06 – 6.97 (m, 1H), 6.91 (d, J = 8.5, 1H), 6.69 (d, J = 2.3, 1H), 5.34 (s, 2H). ^{1}H NMR (400 MHz, Methanol-d_4) δ 7.55 (d, J = 2.3, 1H), 7.12 (d, J = 2.5, 1H), 7.01 (d, J = 8.6, 1H), 6.96 (dd, J = 8.6, 2.5, 1H), 6.73 (d, J = 2.3, 1H), 5.38 (s, 2H). ^{2}H NMR (61 MHz, DMSO) δ 8.13 (s, 1D), 7.37 (s, 1D). ^{13}C NMR (101 MHz, Methanol-d_4) δ 166.6, 158.8, 148.6, 136.9, 133.3, 132.9, 132.3, 129.9 (q, J = 30.6), 129.3 – 128.7 (m), 126.5 – 126.3 (m), 125.6 (q, J = 273.2), 123.5 (q, J = 273.2), 120.0, 113.9 (q, J = 5.9), 99.6, 52.6 (q, J = 2.7). ^{19}F NMR (282 MHz, DMSO-d_6) δ −58.65, −64.39. HRMS *m/z* calculated for $C_{20}H_{10}D_4F_6N_5O_2$ $[M + H]^+$: 474.1297; Found: 474.1288.

7-(Diethylamino)-4-(hydroxymethyl)-2*H*-chromen-2-one (21). SeO_2 (3.33 g, 30.0 mmol) was added to a solution of 7-(diethylamino)-4-methyl-2*H*-chromen-2-one (**20**, 4.7 g, 20.3 mmol) in xylene (120 mL) and the mixture was stirred vigorously and heated to reflux. After 24 h, the heating was stopped and the reaction was continued overnight. The mixture was filtered and concentrated under reduced pressure. The dark brown residual oil was dissolved in EtOH (130 mL), $NaBH_4$ (385 mg, 10.2 mmol) was added and the solution was stirred overnight at room temperature. Thereafter, the suspension was carefully hydrolysed with 1 M HCl, diluted with H_2O and extracted with DCM (3x). The organic phase was washed with brine, dried over Na_2SO_4 and concentrated *in vacuo*. The crude product was purified by column chromatography with DCM (solvent A) and acetone (solvent B) as eluents (gradient: 100 % A to A/B 80:20). This yielded **21** as a yellow solid (1.79 g, 36 %). ^{1}H NMR (300 MHz, DMSO-d_6) δ 7.43 (d, J = 9.0, 1H), 6.66 (dd, J = 9.0, 2.6, 1H), 6.52 (d, J = 2.6, 1H), 6.10 – 6.01 (m, 1H), 5.50 (t, J = 5.6, 1H), 4.66 (dd, J = 5.6, 1.5, 2H), 3.42 (q, J = 7.0, 4H), 1.11 (t, J = 7.0, 6H). ^{13}C NMR (101 MHz, DMSO-d_6) δ 161.1 (s), 156.8 (s), 155.6 (s), 150.2 (s), 125.0 (s), 108.5 (s), 105.7 (s), 103.9 (s), 96.8 (s), 59.0 (s), 43.9 (s), 12.3 (s). HRMS *m/z* calculated for $C_{14}H_{18}NO_3$ $[M + H]^+$: 248.1281; Found: 248.1280.

(7-(Diethylamino)-2-oxo-2*H*-chromen-4-yl)methyl carbonochloridate (22). Alcohol **21** (300 mg, 1.21 mmol) was placed into a Schlenk tube and dissolved in dry THF (2 mL) and cooled to 0 °C. *i*-Pr_2EtN (252 µL, 1.46 mmol) was added and the mixture stirred for 5 min at 0 °C. Triphosgene (360 mg, 1.21 mmol) was pre-dissolved in THF (1 mL) and added via syringe to get an *in situ* produced excess of phosgene in the reaction mixture. Stirring was continued overnight letting the reaction slowly reach room temperature. The reaction mixture was transferred onto a mixture of EtOAc and H_2O (1:1, 100 mL), the layers were separated and the organic layer dried over Na_2SO_4 and filtered. The solvent was removed under reduced pressure and the crude chloroformate **22** further dried in high vacuum. The sensitive product was directly used in the next reaction without further purification.

(7-(Diethylamino)-2-oxo-2H-chromen-4-yl)methyl (4-((3-(2,6-difluorobenzamido)-1*H*-pyrazol-1-yl)methyl)-3-(trifluoromethyl) phenyl) carbonate (23). GSK-7975A (2,6-difluoro-*N*-(1-(4-hydroxy-2-(trifluoromethyl)benzyl)-1*H*-pyrazol-3-yl)benzamide [16]) (120 mg, 0.30 mmol) was transferred into a Schlenk flask and dissolved in a mixture of DCM (3 mL), pyridine (1 mL) and *i*-Pr_2EtN (126 µL), cooled to 0 °C an stirred for 10 min. Subsequently, freshly prepared chloroformate **22** (1.21 mmol) was dissolved in DCM (1 mL) and slowly added creating an excess of 4:1 relative to GSK-7975A. Stirring was continued overnight, allowing the reaction to reach room temperature slowly. As TLC control indicated complete consumption of GSK-7975A, the mixture was treated with 100 mL H_2O/EtOAc (1:1) and the layers were separated. The aqueous layer was extracted with EtOAc (2x), the combined organic layers washed with brine, dried over Na_2SO_4, filtered and the solvent

was evaporated under reduced pressure. Column chromatography (gradient: 100 % A to A/B 65:35) delivered product **23** with bis ((7-(diethylamino)-2-oxo-2*H*-chromen-4-yl)methyl) carbonate (**24**) as a side product. A second column chromatography purification on silica did not remove the side product but rather indicated that the product is not stable using this system. A 2D-TLC test on silica confirmed this assumption. A reversed phase column chromatography on C18 with water (solvent A) and MeCN (solvent B) as eluents was performed instead (gradient: 100 % A to A/B 30:70). The side product could not be removed completely and thus the product was recrystallised to give the title compound as a pale yellow solid (135.6 mg, 67 %). ^{1}H NMR (300 MHz, DMSO-d_6) δ 11.32 (s, 1H), 7.89 (d, J = 2.3, 1H), 7.83 (d, J = 2.5, 1H), 7.63 (dd, J = 8.6, 2.5, 1H), 7.59 – 7.43 (m, 2H), 7.17 (t, J = 8.0, 2H), 7.08 (d, J = 8.6, 1H), 6.71 (dd, J = 9.3, 2.3, 2H), 6.56 (d, J = 2.6, 1H), 6.11 (d, J = 1.1, 1H), 5.51 – 5.44 (m, 4H), 3.44 (q, J = 6.9, 4H), 1.12 (t, J = 6.9, 6H). ^{13}C NMR (101 MHz, DMSO-d_6) δ 160.5, 158.8 (dm, J = 248.4), 157.5, 155.9, 152.1, 150.5, 149.8, 149.0, 147.1, 133.6, 132.1, 132.1 – 131.6 (m), 131.3, 127.3 (q, J = 31.0), 125.8, 125.7, 123.5 (q, J = 274.0), 119.7 – 119.4 (m), 115.5 – 114.2 (m), 112.3 – 111.4 (m), 108.8, 106.0, 105.1, 97.51, 96.9, 65.8, 50.8 (q, J = 4.4, 2.9), 44.0, 12.3. ^{19}F NMR (282 MHz, DMSO-d_6) δ −58.72, −113.98. HRMS *m/z* calculated for $C_{33}H_{28}F_5N_4O_6$ $[M + H]^+$: 671.1924; Found: 671.1927. HRMS *m/z* calculated for side product **24** $C_{29}H_{33}N_2O_7$ $[M + H]^+$: 521.2288; Found: 521.2268.

4.2. Cell culture

All cells were cultured at 37 °C and 5 % CO_2. HEK293T (ATCC® CRL-3216™) and STIM1/STIM2 double knockout HEK293 cells were maintained in culture in 1X DMEM medium (41965-039, ThermoFisher Scientific) supplemented with 10 % FBS, 1 mM sodium pyruvate, 10 mM HEPES, 1X MEM non-essential amino acids and 1 % Penicillin-Streptomycin (P/S). HEK293 cells stably expressing human STIM1 were cultured in MEM medium (ThermoFisher Scientific) supplemented with 10 % FCS and 500 μg/ml G418 (Geneticin) selection antibiotic. HEK293 STIM1 stable cells were further transfected with human Orai1 plasmid DNA according to manufacturer's guidelines in a Nucleofector 4D device with Nucleofector Kit SF (Lonza, Basel, Switzerland) with 1 μg DNA per 10^6 cells. MDA-MB-231 and MCF7 (ATCC) cells were maintained in Gibco™ RPMI 1640 medium (21875-091, ThermoFisher Scientific) supplemented with 10 % FBS, 10 mM HEPES, and 1 % P/S.

4.3. Fluorescent Ca^{2+} influx assay using FLIPR tetra®

The MDA-MB-231, MCF7, and HEK293T cells were seeded in Corning® 96-well black polystyrene clear bottom microplates (CLS3603, Sigma–Aldrich) at a density of 60,000, 30,000, and 55,000, respectively in 100 μl medium per well. Phenol red-free RPMI medium (11835-030, ThermoFisher Scientific) supplemented with 10 % FBS and 10 mM HEPES was used to seed MDA-MB-231 and MCF-7 cells whereas phenol red-free DMEM (31053028, ThermoFisher Scientific) supplemented with 10 % FBS, 4 mM L-Glutamine, 10 mM HEPES, 1 mM sodium pyruvate and 1X MEM non-essential amino acids (11140-050, ThermoFisher Scientific) was used for seeding HEK293T cells for FLIPR. The microplates were coated with 100 μg/mL poly-D-lysine (P6407, Sigma-Aldrich) before seeding the HEK293T or HEK293 STIM1/STIM2 double knockout cells. The HEK293 STIM1/STIM2 double knockout cells were transfected with 200 ng of hOrai1 or hOrai1-ANSGA plasmid DNA per well using Lipofectamine™ 2000 (11668019, ThermoFisher Scientific) at a seeding density of 25,000 cells per well. The $CaCl_2$ concentration in the medium of HEK293 STIM1/STIM2 double knockout cells transfected with hOrai1-ANSGA was limited to approximately 0.2 mM to prevent excessive constitutive Ca^{2+} entry [46].

To assess the effect of GSK-7975A derivatives on SOCE by FLIPR, the growth media of MDA-MB-231, MCF-7 or HEK293T cells was removed 16–20 h after seeding the cells in 96-well microplates. The cells were loaded with 50 μL of the Calcium-5 indicator (FLIPR® Calcium 5 assay kit, R8186, Molecular Devices, Sunnyvale, CA, USA) reconstituted in nominally Ca^{2+} free (NCF) Krebs buffer containing 140 mM NaCl, 4.8 mM KCl, 1 mM $MgCl_2$, 10 mM D-glucose and 10 mM HEPES (pH 7.4) and incubated at 37 °C for 30 min. Following this action, 50 μL of 2X doses of desired concentrations of GSK-7975A or derivatives thereof dissolved in the NCF Krebs buffer were applied on top and incubated for another 30 min at 37 °C. The cells were excited using the internal 470–495 nm LED module of the FLIPR, and the emitted fluorescence signal was filtered with a 515–575 nm emission filter. After recording a 50 s baseline, 50 μL of 3X dose of Thapsigargin (3 μM) dissolved in NCF Krebs buffer was robotically administered to the cells and fluorescence was recorded for 10 min. Following depletion of stores by Thapsigargin, 4X (8 mM) $CaCl_2$ containing Krebs buffer was applied on top of the cells by the robotic arm of FLIPR to initiate SOCE which was recorded for 10 min. To quantify the impact on SOCE by different doses of GSK-7975A and its derivatives, the area under the curve (AUC) of the Ca^{2+} entry traces were calculated using the FLIPR Tetra software, ScreenWorks 3.1.1.8 (Molecular Devices).

To assess the inhibition of constitutive Ca^{2+} entry in hOrai1-ANSGA transfected STIM1/STIM2 double knockout HEK293 cells by GSK-7975A, the 0.2 mM $CaCl_2$ containing DMEM was replaced with 50 μL of the Calcium-5 indicator reconstituted in 0.2 mM $CaCl_2$ containing Krebs buffer and incubated at 37 °C for 30 min. A 2X concentration of 50 μL GSK-7975A also prepared in 0.2 mM $CaCl_2$ containing Krebs buffer was applied per well by the FLIPR robot and incubated for indicated time. Finally, 3X (6 mM) $CaCl_2$ containing Krebs buffer was applied and fluorescence was recorded.

4.4. Electrophysiology

All patch-clamp experiments were performed in a whole-cell patch clamp configuration at 20–24 °C. Currents were acquired and filtered at 2.9 kHz with a HEKA EPC-10 amplifier (HEKA Elektronik, Lambrecht (Pfalz), Germany) and recorded with the HEKA Patchmaster (v2.53) software. Every 2 s, 50 ms voltage ramps spanning from −150 mV to 150 mV were applied from a holding potential of 0 mV. All currents were corrected for a liquid junction potential of 10 mV. Capacitive currents were corrected before every voltage ramp delivery. For analysis, currents at +130 mV and −130 mV were extracted, normalized to cell capacitance and plotted *versus* time. The error bars represent the standard error of mean (SEM). Bath solution contained: 120 mM NaCl, 20 mM $CaCl_2$, 10 mM TEA-Cl, 10 mM HEPES, 2 mM $MgCl_2$. Store-depleting pipette solution contained: 120 mM Cs-glutamate, 20 mM BAPTA, 10 mM HEPES, 3 mM $MgCl_2$, 50 μM IP_3. Osmolarity was adjusted with glucose to 310 mOsm. Under these conditions, pipettes had resistances of 2–3 MΩ.

Transfection: HEK293 cells stably overexpressing STIM1 were harvested at confluency of 70–90 %. 1×10^6 cells were transfected with either 1 μg Orai1 WT (pEGFP-C1-hORAI1 WT), Orai1 Y80E (pEGFP-C1-hORAI1-Y80E generated by site-directed mutagenesis primers - For: 5′-GTC CTG GCG CAA GCT CgA gTT GAG CCG CGC CAA GC-3′ and Rev: 5′-GCT TGG CGC GGC TCA AcT cGA GCT TGC GCC AGG AC-3′) or Orai1 W76E (pEGFP-C1-hORAI1-W76E generated by site-directed mutagenesis primers - For: 5′-CAT GCA GGC GCT GTC Cga GCG CAA GCT CTA CTT G-3′ and Rev: 5′-CAA GTA GAG CTT GCG Ctc GGA CAG CGC CTG CAT G-3′) constructs, with the Nucleofactor SF kit (Lonza, Basel, Switzerland) in the Nucleofactor 4D (Lonza, Basel, Switzerland), according to the manufacturer's protocol. Cells were then seeded on 35 mm dishes and patch-clamp experiments were performed 24–48 h later. Only cells showing comparable (modest) fluorescence levels of EGFP were selected for recordings.

4.5. Photo-crosslinking experiments

STIM1/STIM2 double knockout HEK293 cells seeded in six-well

plates were transiently transfected with eGFP-hOrai1-ANSGA plasmid (2 μg/well). After checking the confluency and transfection under the microscope, the cells were washed twice with 500 μL NCF Krebs buffer. The photo-crosslinking probe was added (40 μM in NCF Krebs buffer) and incubated in the dark at 37 °C for 30 min. The cells were irradiated with 365 nm UV-light (either for 15 min with the 8 W-lamp from ThermoFisher Scientific, product code: 10,231,194, or for 30 s with the custom-build UV LED lamp). Afterwards, the cells were washed again with NCF Krebs buffer (2 × 500 μL), mechanically lysed and the membrane fractions pelleted by centrifugation (200,000 g, 1 h, 4 °C). The pellets were redissolved in buffer (60 μL, 10 mM HEPES, 250 mM sucrose, 0.5 % Triton-X, pH = 7.4), protein concentration estimated by comparison with BSA and adjusted by addition of buffer. These membrane fractions were divided equally, frozen and stored at −20 °C until further use.

For biotinylation of photo-crosslinked proteins via CuAAC ("click chemistry") one membrane fraction aliquot from above was defrosted and diluted with buffer (10 mM HEPES, 250 mM sucrose, 0.5 % Triton-X, pH = 7.4) to get a volume of 55 μL. The following reagents were then added: biotin-PEG_{11}-azide (Sigma Aldrich; 5 μL of a 1.6 mM DMSO stock solution, final concentration of 100 μM), THPTA (tris((1-(3-hydroxypropyl)−1*H*-1,2,3-triazol-4-yl)methyl)amine, 5 μL of a 10 mM aqueous stock solution, final concentration of 625 μM), $CuSO_4$ (5 μL of a 2 mM aqueous stock solution, final concentration of 125 μM) and sodium ascorbate (10 μL of a 80 mM aqueous stock solution, final concentration of 10 mM and a total reaction volume of 80 μL). The reaction mixture was stirred at room temperature for 1 h and dialysed against PBS buffer overnight at 4 °C.

For affinity purification of GFP-fused proteins with GFP-binder beads (product code: gta-100 GFP-Trap_A, ChromoTek Inc., Islandia, NY, USA) the following washing buffer was used: 10 mM Tris (pH 7.5), 150 mM NaCl, 0.5 mM EDTA. GFP-binder beads (suspension of 40 μL) were washed with washing buffer (3 × 700 μM) and spun down after each washing step (3 × 2500 g, 2 min, 4 °C). Washing buffer (400 μL) and protease inhibitor cocktail (PIC) were added to the membrane fraction, everything transferred to the washed beads and incubated for 60 min at 4 °C (rotating samples head-over-tail). The beads were washed with washing buffer (3 × 1 mL) and spun down after each washing step (3 × 2500 g, 2 min, 4 °C). Elution of the GFP-fusion proteins was achieved by heating the resin in SDS-sample buffer (100 μL) for 5 min at 95 °C, followed by centrifugation (2500 g, 2 min, 4 °C) and collection of the supernatant for SDS-PAGE analysis.

In the alternative workflow with the other membrane fraction aliquot, biotinylation of photo-crosslinked, GFP-containing proteins via CuAAC ("click chemistry") was performed on the GFP-binder beads. Beads were loaded with GFP-fused proteins as described above and suspended in buffer (10 mM HEPES, 250 mM sucrose, 0.5 % Triton-X, pH = 7.4) to get a volume of 55 μL. To this suspension were added the following reagents: biotin-PEG_{11}-azide (Sigma Aldrich; 5 μL of a 1.6 mM DMSO stock solution, final concentration of 100 μM), THPTA (tris ((1-(3-hydroxypropyl)-1*H*-1,2,3-triazol-4-yl)methyl)amine, 5 μL of a 10 mM aqueous stock solution, final concentration of 625 μM), $CuSO_4$ (5 μL of a 2 mM aqueous stock solution, final concentration of 125 μM) and sodium ascorbate (10 μL of a 80 mM aqueous stock solution, final concentration of 10 mM and a total reaction volume of 80 μL). The suspension was stirred at room temperature for 1 h and the beads washed three times with PBS buffer. GFP-fusion proteins were eluted from the beads as described above.

4.6. Protein mass spectrometry

The cut out SDS-PAGE gel band pieces were reduced, alkylated and digested with different enzymes (trypsin, proteinase K, endoproteinase Glu-C or thermolysin). The digests were analysed by liquid chromatography (LC)-MS/MS (PROXEON coupled to a QExactive HF mass spectrometer, ThermoFisher Scientific) with one injection of 5 μL digests. Peptides were trapped on a μPrecolumn C18 PepMap100 (5 μm, 100 A, 300 μm × 5 mm, ThermoFisher Scientific, Reinach, Switzerland) and separated by backflush on a C18 column (5 μm, 100 A, 75 μm × 15 cm, C18) by applying a 40-minute gradient of 5 % acetonitrile to 40 % in water, 0.1 % formic acid, at a flow rate of 300 nL/min. The Full Scan method was set with resolution at 60,000 with an automatic gain control (AGC) target of 1E06 and maximum ion injection time of 50 ms. The data-dependent method for precursor ion fragmentation was applied with the following settings: resolution 15,000, AGC of 1E05, maximum ion time of 110 milliseconds, mass window 1.6 *m/z*, collision energy 27, under fill ratio 1 %, charge exclusion of unassigned and 1^+ ions, and peptide match preferred, respectively. Spectra interpretation was performed with Proteome Discoverer 2.3 against a human database, using fixed modifications of carboamidomethylated on Cys, and variable modification of oxidation on Met, **5** and **5**-d_4 on different amino acids and acetylation on protein *N*-Term. Parent and fragment mass tolerances were set to 10 ppm and 0.4 Da, respectively. Matches on the reversed sequence database were used to set a Z-score threshold, where 1 % false discoveries on the peptide spectrum match level had to be expected. Protein identifications were only accepted, when two unique peptides fulfilling the 1 % FDR criterion were identified.

4.7. Data analysis

Statistical significance between the two groups was estimated using student's T-test where both groups were normally distributed and Mann Whitney test in case of data that were not distributed normally, unless otherwise noted. GraphPad Prism v8.4.3 was used to perform the statistical analysis as well as to generate the bar graphs with scattered individual data points. Data are usually shown as mean ± SD.

CRediT authorship contribution statement

Dominic Tscherrig: Conceptualization, Methodology, Validation, Formal analysis, Investigation, Visualization, Writing – review & editing. **Rajesh Bhardwaj:** Conceptualization, Methodology, Validation, Formal analysis, Investigation, Visualization, Writing – review & editing. **Daniel Biner:** Investigation. **Jan Dernič:** Investigation. **Daniela Ross-Kaschitza:** Investigation, Formal analysis, Visualization. **Christine Peinelt:** Validation, Formal analysis, Visualization, Writing – review & editing, Supervision. **Matthias A. Hediger:** Supervision, Project administration, Funding acquisition. **Martin Lochner:** Conceptualization, Methodology, Validation, Formal analysis, Writing – original draft, Writing – review & editing, Visualization, Supervision, Project administration, Funding acquisition.

Declaration of Competing Interest

The authors declare no conflict of interest with the contents of this article. The funder had no role in the design of the study, the collection, analyses, or interpretation of data, the writing of the manuscript, or in the decision to publish the results.

Data availability

Data will be made available on request.

Acknowledgements

This work was supported by the Swiss National Science Foundation [Sinergia grants CRSII3_160782 and CRSII5_180326] to M. A. H and M. L. R. B. was also supported by the Marie Curie Actions International Fellowship Program IFP TransCure, University of Bern, Switzerland (from 2014 to 2017). We thank the analytical services from the Department of Chemistry, Biochemistry and Pharmaceutical Sciences

(DCBP), University of Bern, Switzerland, for measuring the spectra of synthetic compounds: the group of Prof. Julien Furrer for measuring NMR spectra, and the group of Prof. Stefan Schürch for MS and HRMS spectra. We thank René Schraner from the DCBP electronics workshop for building the custom-made LED irradiation lamp. We thank Roland Baur for conducting electrophysiology recordings with photo-caged GSK-7975A, Dr. Gergely Gyimesi for providing the hOrai1 homology model and Sophie Braga-Lagache and Prof. Manfred Heller (Core Facility Proteomics & Mass Spectrometry, Department of BioMedical Research, University of Bern, Switzerland) for conducting the protein MS/MS experiments. We also thank Prof. Nicolas Demaurex for providing the His_6-tagged human Orai1 mammalian transfection construct and Dr. Giuseppe Albano for helping with preparation of cellular membrane fractions.

Supplementary materials

Supplementary material associated with this article can be found, in the online version, at doi:10.1016/j.ceca.2023.102834.

References

[1] M. Prakriya, R.S. Lewis, Store-operated calcium channels, Physiol. Rev. 95 (2015) 1383–1436, https://doi.org/10.1152/physrev.00020.2014.
[2] N.T. Nguyen, W. Han, W.M. Cao, et al., Store-operated calcium entry mediated by ORAI and STIM, Compr. Physiol. 8 (2018) 981–1002, https://doi.org/10.1002/cphy.c170031.
[3] J. Avila-Medina, I. Mayoral-Gonzalez, A. Dominguez-Rodriguez, et al., The complex role of store operated calcium entry pathways and related proteins in the function of cardiac, skeletal and vascular smooth muscle cells, Front. Physiol. 9 (2018) 257, https://doi.org/10.3389/fphys.2018.00257.
[4] Y.-J. Park, S.-A. Yoo, M. Kim, W.-U. Kim, The role of calcium–calcineurin–NFAT signaling pathway in health and autoimmune diseases, Front. Immunol. 11 (2020) 195, https://doi.org/10.3389/fimmu.2020.00195.
[5] A. Secondo, G. Bagetta, D. Amantea, On the role of store-operated calcium entry in acute and chronic neurodegenerative diseases, Front. Mol. Neurosci. 11 (2018) 87, https://doi.org/10.3389/fnmol.2018.00087.
[6] Y.F. Chen, P.C. Lin, Y.M. Yeh, L.H. Chen, M.R. Shen, Store-operated Ca^{2+} entry in tumor progression: from molecular mechanisms to clinical implications, Cancers (Basel) 11 (2019) 899, https://doi.org/10.3390/cancers11070899.
[7] L. Waldherr, A. Tiffner, D. Mishra, et al., Blockage of store-operated Ca^{2+} influx by Synta66 is mediated by direct inhibition of the Ca^{2+} selective Orai1 pore, Cancers (Basel) 12 (2020) 2876, https://doi.org/10.3390/cancers12102876.
[8] K.T. Ma, B.C. Guan, Y.Q. Yang, A.L. Nuttall, Z.G. Jiang, 2-Aminoethoxydiphenyl borate blocks electrical coupling and inhibits voltage-gated K^+ channels in guinea pig arteriole cells, Am. J. Physiol.: Heart Circ. Physiol. 300 (2011) H335–H346, https://doi.org/10.1152/ajpheart.00737.2010.
[9] D. Bai, C. del Corsso, M. Srinivas, D.C. Spray, Block of specific gap junction channel subtypes by 2-aminoethoxydiphenyl borate (2-APB), J. Pharmacol. Exp. Ther. 319 (2006) 1452–1458, https://doi.org/10.1124/jpet.106.112045.
[10] H.T. Ma, K. Venkatachalam, H.S. Li, et al., Assessment of the role of the inositol 1,4,5-trisphosphate receptor in the activation of transient receptor potential channels and store-operated Ca^{2+} entry channels, J. Biol. Chem. 276 (2001) 18888–18896, https://doi.org/10.1074/jbc.M100944200.
[11] H.Z. Hu, Q. Gu, C. Wang, et al., 2-aminoethoxydiphenyl borate is a common activator of TRPV1, TRPV2, and TRPV3, J. Biol. Chem. 279 (2004) 35741–35748, https://doi.org/10.1074/jbc.M404164200.
[12] G. Kovacs, N. Montalbetti, A. Simonin, et al., Inhibition of the human epithelial calcium channel TRPV6 by 2-aminoethoxydiphenyl borate (2-APB), Cell Calcium 52 (2012) 468–480, https://doi.org/10.1016/j.ceca.2012.08.005.
[13] A. Hofer, G. Kovacs, A. Zappatini, M. Leuenberger, M.A. Hediger, M. Lochner, Design, synthesis and pharmacological characterization of analogs of 2-aminoethyl diphenylborinate (2-APB), a known store-operated calcium channel blocker, for inhibition of TRPV6-mediated calcium transport, Bioorg. Med. Chem. 21 (2013) 3202–3213, https://doi.org/10.1016/j.bmc.2013.03.037.
[14] E.J. Slowik, K. Stankoska, N.N. Bui, et al., The calcium channel modulator 2-APB hydrolyzes in physiological buffers and acts as an effective radical scavenger and inhibitor of the NADPH oxidase 2, Redox Biol. 61 (2023), 102654, https://doi.org/10.1016/j.redox.2023.102654.
[15] X. Zhang, P. Xin, R.E. Yoast, et al., Distinct pharmacological profiles of ORAI1, ORAI2, and ORAI3 channels, Cell Calcium 91 (2020), 102281, https://doi.org/10.1016/j.ceca.2020.102281.
[16] A. Schild, R. Bhardwaj, N. Wenger, et al., Synthesis and pharmacological characterization of 2-aminoethyl diphenylborinate (2-APB) derivatives for inhibition of store-operated calcium entry (SOCE) in MDA-MB-231 breast cancer cells, Int. J. Mol. Sci. 21 (2020) 5604, https://doi.org/10.3390/ijms21165604.
[17] H. Schleifer, B. Doleschal, M. Lichtenegger, et al., Novel pyrazole compounds for pharmacological discrimination between receptor-operated and store-operated Ca^{2+} entry pathways, Br. J. Pharmacol. 167 (2012) 1712–1722, https://doi.org/10.1111/j.1476-5381.2012.02126.x.
[18] R. Takezawa, H. Cheng, A. Beck, et al., A pyrazole derivative potently inhibits lymphocyte Ca^{2+} influx and cytokine production by facilitating transient receptor potential melastatin 4 channel activity, Mol. Pharmacol. 69 (2006) 1413–1420, https://doi.org/10.1124/mol.105.021154.
[19] I. Derler, R. Schindl, R. Fritsch, et al., The action of selective CRAC channel blockers is affected by the Orai pore geometry, Cell Calcium 53 (2013) 139–151, https://doi.org/10.1016/j.ceca.2012.11.005.
[20] G. Chen, S. Panicker, K.-Y. Lau, et al., Characterization of a novel CRAC inhibitor that potently blocks human T cell activation and effector functions, Mol. Immunol. 54 (2013) 355–367, https://doi.org/10.1016/j.molimm.2012.12.011.
[21] M. Serafini, C. Cordero-Sanchez, R. Di Paola, et al., Store-operated calcium entry as a therapeutic target in acute pancreatitis: discovery and development of drug-like SOCE inhibitors, J. Med. Chem. 63 (2020) 14761–14779, https://doi.org/10.1021/acs.jmedchem.0c01305.
[22] N.R. Khedkar, N.R. Irlapatti, D. Dadke, et al., Discovery of a novel potent and selective calcium release-activated calcium channel inhibitor: 2,6-difluoro-*N*-(2′-methyl-3′-(4-methyl-5-oxo-4,5-dihydro-1,3,4-oxadiazol-2-yl)-[1,1′-biphenyl]-4-yl) benzamide. Structure–activity relationship and preclinical characterization, J. Med. Chem. 64 (2021) 17004–17030, https://doi.org/10.1021/acs.jmedchem.1c01403.
[23] F.M. Hannan, V.N. Babinsky, R.V. Thakker, Disorders of the calcium-sensing receptor and partner proteins: insights into the molecular basis of calcium homeostasis, J. Mol. Endocrinol. 57 (2016) R127–R142, https://doi.org/10.1530/jme-16-0124.
[24] J. Kniazeff, L. Prézeau, P. Rondard, J.-P. Pin, C. Goudet, Dimers and beyond: the functional puzzles of class C GPCRs, Pharmacol. Ther. 130 (2011) 9–25, https://doi.org/10.1016/j.pharmthera.2011.01.006.
[25] A.D. Conigrave, S.J. Quinn, E.M. Brown, L-Amino acid sensing by the extracellular Ca^{2+}-sensing receptor, Proc. Natl. Acad. Sci. U. S. A. 97 (2000) 4814–4819, https://doi.org/10.1073/pnas.97.9.4814.
[26] K. Hüll, J. Morstein, D. Trauner, *In vivo* photopharmacology, Chem. Rev. 118 (2018) 10710–10747, https://doi.org/10.1021/acs.chemrev.8b00037.
[27] P. Klán, T. Šolomek, C.G. Bochet, et al., Photoremovable protecting groups in chemistry and biology: reaction mechanisms and efficacy, Chem. Rev. 113 (2013) 119–191, https://doi.org/10.1021/cr300177k.
[28] N.R. Burton, P. Kim, K.M. Backus, Photoaffinity labelling strategies for mapping the small molecule–protein interactome, Org. Biomol. Chem. 19 (2021) 7792–7809, https://doi.org/10.1039/D1OB01353J.
[29] R. Udasin, A. Sil, E. Zomot, et al., Photopharmacological modulation of native CRAC channels using azoboronate photoswitches, Proc. Natl. Acad. Sci. U. S. A. 119 (2022), e2118160119, https://doi.org/10.1073/pnas.2118160119.
[30] X. Yang, G. Ma, S. Zheng, et al., Optical control of CRAC channels using photoswitchable azopyrazoles, J. Am. Chem. Soc. 142 (2020) 9460–9470, https://doi.org/10.1021/jacs.0c02949.
[31] S. Kiyonaka, K. Kato, M. Nishida, et al., Selective and direct inhibition of TRPC3 channels underlies biological activities of a pyrazole compound, Proc. Natl. Acad. Sci. U. S. A. 106 (2009) 5400–5405, https://doi.org/10.1073/pnas.0808793106.
[32] K.-S. Lee, K.-D. Kim, A convenient and efficient method for demethylation of aryl methyl ethers with magnesium iodide in ionic liquid, Bull. Korean Chem. Soc. 31 (2010) 3842–3843, https://doi.org/10.5012/bkcs.2010.31.12.3842.
[33] A. Novak, L.D. Humphreys, M.D. Walker, S. Woodward, Amide bond formation using an air-stable source of $AlMe_3$, Tetrahedron Lett. 47 (2006) 5767–5769, https://doi.org/10.1016/j.tetlet.2006.06.004.
[34] V.V. Rostovtsev, L.G. Green, V.V. Fokin, K.B. Sharpless, A stepwise Huisgen cycloaddition process: copper(I)-catalyzed regioselective "ligation" of azides and terminal alkynes, Angew. Chem. Int. Ed. 41 (2002) 2596–2599, https://doi.org/10.1002/1521-3773(20020715)41:14<2596::AID-ANIE2596>3.0.CO;2-4.
[35] T.R. Chan, R. Hilgraf, K.B. Sharpless, V.V. Fokin, Polytriazoles as copper(I)-stabilizing ligands in catalysis, Org. Lett. 6 (2004) 2853–2855, https://doi.org/10.1021/ol0493094.
[36] S.M. Lamos, C.J. Krusemark, C.J. McGee, M. Scalf, L.M. Smith, P.J. Belshaw, Mixed isotope photoaffinity reagents for identification of small-molecule targets by mass spectrometry, Angew. Chem. Int. Ed. 45 (2006) 4329–4333, https://doi.org/10.1002/anie.200600743.
[37] Z. Song, W. Huang, Q. Zhang, Isotope-coded, fluorous photoaffinity labeling reagents, Chem. Commun. 48 (2012) 3339–3341, https://doi.org/10.1039/C2CC00027J.
[38] B.D. Kesling, B.C. Söderberg, T. Gullion, Synthesis of isotopically labeled tri-*p*-tolylamine, J. Labelled Compd. Radiopharm. 43 (2000) 1059–1068, https://doi.org/10.1002/1099-1344(200009)43:10<1059::AID-JLCR392>3.0.CO;2-D.
[39] L. Zhang, Y. Zhang, J. Dong, J. Liu, L. Zhang, H. Sun, Design and synthesis of novel photoaffinity probes for study of the target proteins of oleanolic acid, Bioorg. Med. Chem. Lett. 22 (2012) 1036–1039, https://doi.org/10.1016/j.bmcl.2011.11.123.
[40] P. Wang, Photolabile protecting groups: structure and reactivity, Asian J. Org. Chem. 2 (2013) 452–464, https://doi.org/10.1002/ajoc.201200197.
[41] A. Nadler, G. Reither, S. Feng, et al., The fatty acid composition of diacylglycerols determines local signaling patterns, Angew. Chem. Int. Ed. 52 (2013) 6330–6334, https://doi.org/10.1002/anie.201301716.
[42] R.O. Schönleber, J. Bendig, V. Hagen, B. Giese, Rapid photolytic release of cytidine 5′-diphosphate from a coumarin derivative: a new tool for the investigation of ribonucleotide reductases, Bioorg. Med. Chem. 10 (2002) 97–101, https://doi.org/10.1016/S0968-0896(01)00254-1.

[43] J.E. Horne, M. Walko, A.N. Calabrese, et al., Rapid mapping of protein interactions using tag-transfer photocrosslinkers, Angew. Chem. Int. Ed. 57 (2018) 16688–16692, https://doi.org/10.1002/anie.201809149.
[44] J. Babin, M. Pelletier, M. Lepage, J.-F. Allard, D. Morris, Y. Zhao, A new two-photon-sensitive block copolymer nanocarrier, Angew. Chem. Int. Ed. 48 (2009) 3329–3332, https://doi.org/10.1002/anie.200900255.
[45] Y. Zhou, X. Cai, N.A. Loktionova, et al., The STIM1-binding site nexus remotely controls Orai1 channel gating, Nat. Commun. 7 (2016) 13725, https://doi.org/10.1038/ncomms13725.
[46] B. Augustynek, G. Gyimesi, J. Dernič, et al., Discovery of novel gating checkpoints in the Orai1 calcium channel by systematic analysis of constitutively active mutants of its paralogs and orthologs, Cell Calcium 105 (2022), 102616, https://doi.org/10.1016/j.ceca.2022.102616.
[47] T. Jack, M. Leuenberger, M.-D. Ruepp, et al., Mapping the orthosteric binding site of the human 5-HT_3 receptor using photo-cross-linking antagonists, ACS Chem. Neurosci. 10 (2019) 438–450, https://doi.org/10.1021/acschemneuro.8b00327.
[48] X. Hou, L. Pedi, M.M. Diver, S.B. Long, Crystal structure of the calcium release-activated calcium channel Orai, Science 338 (2012) 1308–1313, https://doi.org/10.1126/science.1228757.
[49] M. Nassal, 4-(1-Azi-2,2,2-trifluoroethyl)benzoic acid, a highly photolabile carbene generating label readily fixable to biochemical agents, Liebigs Ann. Chem. 1983 (1983) 1510–1523, https://doi.org/10.1002/jlac.198319830907.
[50] K.A.H. Chehade, H.P. Spielmann, Facile and efficient synthesis of 4-azidotetrafluoroaniline: a new photoaffinity reagent, J. Org. Chem. 65 (2000) 4949–4953, https://doi.org/10.1021/jo000402p.